SYSTEMATIC ANALYSIS OF GENETIC AND PHARMACEUTICAL MODULATORS OF THE EUKARYOTIC CELL CYCLE

A Dissertation

by

SCOTT ALLEN HOOSE

Submitted to the Office of Graduate Studies of
Texas A&M University
in partial fulfillment of the requirements for the degree of

DOCTOR OF PHILOSOPHY

August 2012

Major Subject: Biochemistry

Systematic Analysis of Genetic and Pharmaceutical Modulators of the Eukaryotic Cell Cycle

SYSTEMATIC ANALYSIS OF GENETIC AND PHARMACEUTICAL MODULATORS OF THE EUKARYOTIC CELL CYCLE

A Dissertation

by

SCOTT ALLEN HOOSE

Submitted to the Office of Graduate Studies of
Texas A&M University
in partial fulfillment of the requirements for the degree of

DOCTOR OF PHILOSOPHY

Approved by:

Chair of Committee, Michael Polymenis
Committee Members, Mary Bryk
Feng Qiao
Matthew Sachs
Head of Department, Gregory Reinhart

August 2012

Major Subject: Biochemistry

ABSTRACT

Systematic Analysis of Genetic and Pharmaceutical Modulators of the Eukaryotic Cell Cycle. (August 2012)

Scott Allen Hoose, B.A., Texas A&M University

Chair of Advisory Committee, Dr. Michael Polymenis

Cell replication and division are central to the proliferation of life, and have implications for normal growth and development as well as disease state. Assembly of a complete picture of the systems which control this process requires identification of individual genetic components, but the identity and complete sequence of events that trigger initiation of cell division, at a point called START in yeast, remain unknown. Here, we evaluated panels of non-essential single gene deletion strains and tested the effects of FDA-approved drugs on cell-cycle progression, using flow cytometry to detect altered DNA content.

Previous studies relied mainly on cell size changes to systematically identify genes required for the timely completion of START. This analysis revealed that most gene deletions that altered cell-cycle progression did not change cell size. Our results highlight a strong requirement for ribosomal biogenesis and protein synthesis for initiation of cell division. We also identified numerous factors that have not been previously implicated in cell-cycle control mechanisms. We found that cystathionine-β-synthase (CBS) advances START in two ways: by promoting cell growth, which

requires CBS's catalytic activity, and by a separate function which does not require that activity. CBS defects cause disease in humans, and in animals CBS has vital, non-catalytic, unknown roles. Hence, our results may be relevant for human biology.

Screening chemical libraries to identify compounds that affect overall cell proliferation is common. However, it is generally not known whether the compounds tested alter the timing of particular cell-cycle transitions. Our approach revealed strong cell-cycle effects of several commonly used pharmaceuticals. We show that the antilipemic gemfibrozil delays initiation of DNA replication, while cells treated with the antidepressant fluoxetine severely delay progression through mitosis. We discovered a strong suppressive interaction between gemfibrozil and fluoxetine. The novel interaction between gemfibrozil and fluoxetine suggests that identifying and combining drugs that show cell-cycle effects might streamline identification of drug combinations with a pronounced impact on cell proliferation.

Our studies not only transform our view of START, but also expand the repertoire of genetic and chemical means to modulate the eukaryotic cell cycle.

DEDICATION

To Julianne,
our children,
and our parents,
all of whom are a constant and happy reminder
to me of why life is important
and worth understanding

ACKNOWLEDGEMENTS

I would like to sincerely thank my advisor, Dr. Michael Polymenis, for his support, friendship, and for the opportunity he gave me to collaborate on and help build several very highly productive and enjoyable years of research. I'm grateful to our research team, without whom this project would have been impossible, to Dr. Roger Smith for his collaboration and assistance with flow cytometry, and to John J. Pearce, Jr for helpful advice on data organization strategies. I thank the members of my committee, Dr. Mary Bryk, Dr. Feng Qiao, and Dr. Matthew Sachs for their encouragement and advice, and Dr. Michael Kladde and Dr. C. Cheng Kao, who helped me to get started and move forward in science.

My thanks also to the Department of Biochemistry and Biophysics for the assistance and the assistantships, to Drs. Chandler, Pettigrew, Ayres, Park, Funkhouser, and Miles for the opportunity to teach with them, to my many students who made the teaching rewarding, to my colleagues who have been a source of friendship and support, and to Texas A&M University and the National Science Foundation for research funding.

Lastly, my thanks to my family, who have supported me always.

TABLE OF CONTENTS

LIST OF FIGURES

1. INTRODUCTION AND LITERATURE REVIEW*

"Omnis cellula e cellula" ("Every cell from a cell")

- François-Vincent Raspail, popularized by Rudolph Carl Virchow, 1858

All life as we know it is physically organized into autonomous or semi-autonomous membrane-bound structures called cells. The phrase above was coined at a time when the scientific community had just begun to accept the concept that cells do not, and in fact cannot, arise spontaneously from non-cellular precursors, but rather must be generated from pre-existing cells through a process of division. Debate of whether simpler structures by definition should be considered *life* is beyond the scope of this thesis, but it nevertheless holds true that even in the cases of the prototypical example of viruses, interaction with cellular life is required in order to proliferate. Thus, even though specifics of cellular structure and role vary widely across diverse phylogenetic taxa and even from tissue to tissue within individual higher-order organisms, the requirement for a cellular progenitor is an axiom for cell origination, and by extension the proliferation of all life. In addition, the mechanisms by which eukaryotic cells

---

This dissertation follows the style of Molecular and Cellular Biology.
*Major portions of this dissertation have been adapted from *Hoose SA et al. 2012. A systematic analysis of cell cycle regulators in yeast reveals that most factors act independently of cell size to control initiation of division. PLoS Genet. Mar;8(3): e1002590. Epub 2012 Mar 15* and *Hoose SA et al. 2012. Systematic analysis of cell cycle effects of common drugs leads to the discovery of a suppressive interaction between gemfibrozil and fluoxetine. PLoS One 7(5): e36503.*

accomplish that division are often highly conserved. Therefore, an accurate and complete understanding of the systems which comprise and regulate the replicative process could arguably be considered central to our understanding of life itself.

Cells contain or can synthesize the internal structures and molecular machinery required for them to replicate through division. Subcellular components must also be replicated, and, as in the case of any complex constructive process, there exist systems which gather the necessary resources, assess the current state of the system, commit to the process, produce or organize the machinery specific to replication and division, and then subsequently initiate the process at the proper time and place. Throughout the regimen, components of these and other pathways must be appropriately activated and/or deactivated, in response to specific internal and external stimuli. As with most aspects of cellular life, the replicative program is encoded at its highest level in the genetic material of the cell, resulting in the expression of factors which may themselves serve to regulate the expression of other genes or effect other metabolic, structural, or regulatory changes to the cell environment. Thus, it is important, so far as we are currently able, to define the contributions of individual genes to this process. This initially requires experimental identification of those genes which impact it most significantly. Much is currently known about the cell cycle, the program by which a cell prepares to divide and then undergoes division, in the process giving rise to one or more daughter cells, but science demands that existing models and paradigms be expanded and re-evaluated as additional data becomes available.

In multicellular organisms, proper regulation of cell growth and division is critical for proper tissue/organ growth and development, as well as regenerative capabilities, for example, in wound healing. Disruption of the proper progression of this program can result in termination of the process, death of the cell, or misregulated or even unregulated division. These effects can manifest themselves as a pathology, such as cancer. From a basic scientific standpoint, we seek ultimately to fully understand the endogenous systems: how they are organizationally structured, how they respond to various differential environmental and metabolic stimuli, and how defects in those systems affect phenotype. From a medical or engineering perspective, we seek effective ways to manipulate that process, either in therapeutic response to disrupted or diseased state, or as prophylaxis. In this thesis, we expand the body of knowledge relative both to the basic understanding of the natural process and to possibilities of its modulation, using the yeast *Saccharomyces cerevisiae* as a model organism.

S. cerevisiae is an important eukaryotic model for many reasons, including ease of culture and availability of a wide variety of genetic and bioinformatic resources. These include the entire sequence of the yeast genome, and commercial gene deletion panels for both diploid and haploid strains which cover the vast majority (>90%) of the genome. Most importantly, many key discoveries pertaining to higher-order eukaryotes have been made through study of yeast homologs. General cell organization and mitotic cell-cycle progression are highly conserved from yeast to humans; in fact, the yeast and human homologs of the central regulator of the cell cycle, the cyclin-dependent kinase Cdk1 (yeast gene *CDC28*, human *CDC2*), share 60-65% sequence similarity, and human

Cdc2 can complement the yeast *cdc28* mutation. The cell cycle consists of multiple phases: a) interphase, which includes Gap 1 (G1), Synthesis (S), and Gap 2 (G2) subphases, during which the cell assesses its status and commits to replication (G1) and synthesizes a copy of its DNA (S), and b) mitosis, during which the cell divides. Thus, by definition, progression from G1 to G2 is delineated by DNA synthesis, and measurement of DNA content of the cell is the most fundamental indicator of the cell-cycle phase it currently occupies.

Understanding cell division requires knowing not only *how*, but also what determines *when* cells divide. Previous studies identified several components of the machinery that drives the cell cycle. However, it is not clear how cellular pathways impinge on the cell division machinery to initiate cell division. This is a critical gap in our understanding, since this process governs overall proliferation: once cells initiate their division, they are committed to completing it.

In proliferating cells, the G1 phase of any given cell cycle lasts from the end of the previous mitosis until the beginning of DNA synthesis. In unfavorable growth conditions, eukaryotic cells typically stay longer in G1, delaying initiation of DNA replication (5, 15, 42, 48, 50, 83, 97). Subsequent cell-cycle transitions, culminating with mitosis, are less sensitive to growth limitations, and their timing does not vary greatly, even if growth conditions worsen. Hence, differences in the length of the G1 phase account for most of the differences in total cell cycle, or generation times, between the same cells growing in different media, or among different cells of the same organism. Such fundamental observations support the notion that eukaryotic cells commit to a new

round of cell division at some point in late G1 (5, 50, 75, 76). Budding yeast cells also evaluate their "growth" in late G1 at a point called START, before DNA synthesis in S phase (83). In favorable growth conditions, and in the absence of mating pheromones (for haploids), or meiotic inducers (for diploids), cells pass through START (83). Passage through START and commitment to cell division precedes a large transcriptional program and additional events that lead to initiation of DNA replication (25, 30, 96).

The lack of a detailed view of upstream regulatory networks that govern the timing of START in the yeast *Saccharomyces cerevisiae* is surprising, given the rich history of the field. The classic *cdc* screen identified factors essential for START, such as Cdc28p (83), the main yeast cyclin-dependent kinase (Cdk). However, the *cdc* screen did not target nonessential regulators, such as the cyclin regulatory subunits of Cdc28p (8). Other efforts relied on gene-specific suppression (28, 39, 40, 85, 103) or sensitivity to mating pheromones (21, 26). By far, however, most approaches to identify regulators of START interrogated cell size. Almost half a century ago, a relationship between the size or mass of a cell and the timing of initiation of DNA replication was described from bacterial (24), to mammalian cells (58). Indeed, a newborn budding yeast cell is smaller than its mother is, and it will not initiate cell division without first increasing in size (83). Thus, it appears that there is a critical size threshold for START completion in yeast. Based on this concept of a critical size, the question of "*when* do cells divide?" was reduced to "*what size* are cells when they divide?" Hence, several screens for regulators of START interrogated cell size (16, 52, 82, 102, 120). In fact, systematic, genome-wide

approaches to find genes required for the correct timing of START relied solely on cell size changes (52, 120).

Any gene deletion that alters the length of the G1 phase relative to the rest of the phases of the cell cycle will alter the DNA content profile. Thus, the DNA content of a population reports on the relative length of the G1 phase directly, by identifying the fraction of cells with unreplicated genome. In yeast, DNA content analyses measured the effects of gene over-expression on cell-cycle progression (70, 101), or cycle arrest when essential genes were turned-off (118). However, the yeast single-gene deletion collections have not been evaluated with this method.

To assess cell-cycle progression more directly, we evaluated by flow cytometry the yeast deletion collection of nonessential genes for altered DNA content. We found that most gene deletions that altered cell-cycle progression did not change cell size. Our results suggest that evaluating the length of the G1 phase of the cell cycle, instead of cell size, provides a much more accurate view of the contribution of individual gene products to the timing of START and commitment to cell division. We also documented a strong requirement for ribosomal biogenesis for initiation of cell division, and identified numerous factors that have not been implicated previously in cell-cycle control mechanisms. One such factor is the metabolic enzyme cystathionine-β-synthase (CBS; Cys4p in yeast). We discovered a novel, non-catalytic role of CBS in accelerating START.

Taken together, the data we present here substantially expand the range of factors that affect initiation of cell division. We discuss the significance of our finding that most

gene deletions that change the length of the G1 phase do not alter cell size, in the context of models that center on the role of cell size at START.

Adjusting rates of cell proliferation is the objective of many therapeutic strategies. Most often, the goal is to impede or block cell proliferation of target cells, as with chemotherapy in cancer. In other cases, as in tissue regeneration, the goal is to promote cell proliferation. Proliferating eukaryotic cells pass through a series of highly regulated cell-cycle phases, culminating with mitosis (83). Hence, drugs that influence the timing of cell-cycle transitions are useful in efforts to adjust rates of cell proliferation.

Identifying drugs that potentiate the effects of other drugs is the leading therapeutic strategy in the treatment of numerous diseases, such as cancer (93), tuberculosis (13) and HIV-AIDS (79). Conversely, drug interactions may suppress a desired response, or even lead to a harmful outcome. Screening libraries composed of a few hundred thousand compounds for a sought-after effect of a single chemical is now common (46). However, testing all the possible combinations, even binary ones, of these chemicals represents a formidable obstacle (10).

Here we report a systematic analysis of cell-cycle progression of yeast cells exposed to a panel of FDA-approved drugs. We document novel cell-cycle effects of several compounds. We also reasoned that drugs that affect cell-cycle progression might be more likely to display interactions with other such drugs, and thereby greatly impact overall cell proliferation. We demonstrate one such novel drug interaction, between gemfibrozil and fluoxetine.

2. RESULTS

2.1 Genetic deletion analysis

Rationale and outline of the experimental design. We measured the DNA content during exponential growth in rich media (YPD-2% dextrose (55), see Materials and Methods), for several reasons: First, exponential growth in liquid media affords much greater reproducibility (90). Second, for the haploid deletion strains, cell size measurements during the same growth conditions are available (52). Third, fitness data during growth in the same rich media are available (35), providing another parameter for interpreting our findings.

We used the homozygous diploid deletion panel to query the nonessential genes, to minimize the effects of aneuploidy found in a substantial portion of haploid deletion strains (47). We evaluated strains individually (Fig. 1). We quantified each sample in an automated manner, recording the percentage of cells with unreplicated genome (%G1, see Materials and Methods). We did not quantify complex profiles (e.g., due to cell separation defects, see Fig. A-1), and we excluded these strains from further analyses. At the beginning and end of most batches of strains, we measured the reference wild type strain (BY4743), which was cultured and processed along with the deletion strains. To identify strains with altered cell cycle, we compared the frequency distribution of the deletion strains against a normal distribution fit of the wild type (31.17% ±5.20, n=250) samples (Fig. 2). Deletion strains that had a %G1 greater or less than two standard

deviations of the wild-type distribution were considered to differ significantly from wild type, and we evaluated them further (see Materials and Methods).

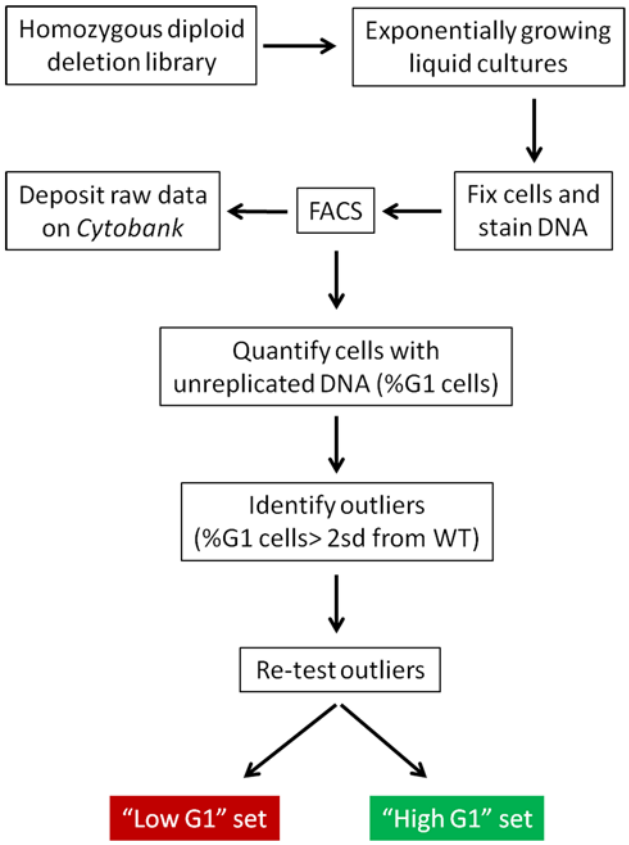

FIG 1 Schematic overview of our approach. For a detailed description of all the protocols we used, see Materials and Methods.

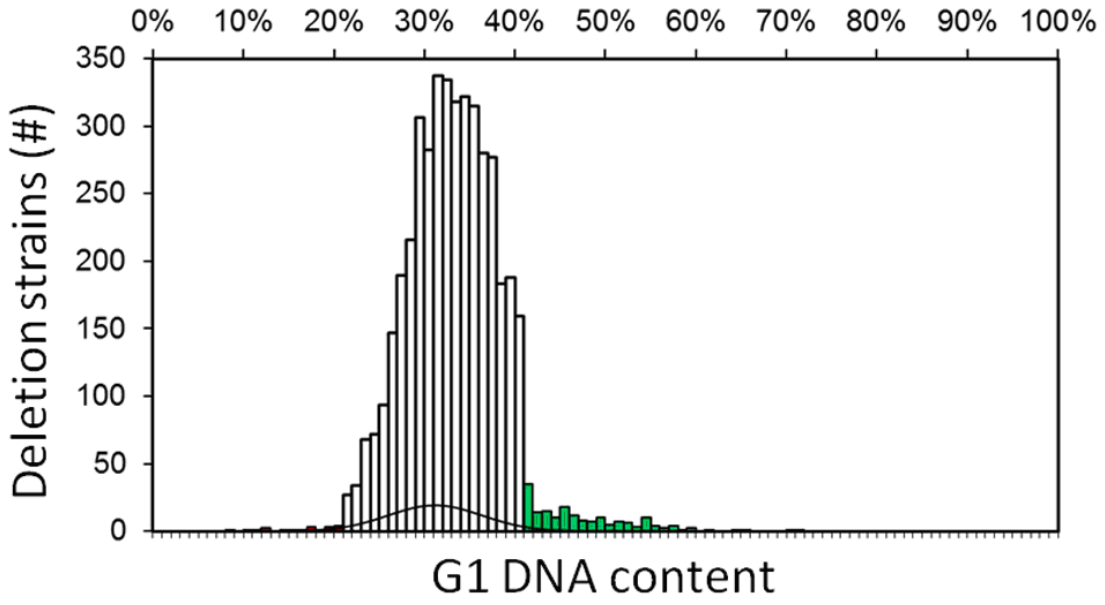

FIG 2 DNA content screen identifies genes required for normal cell-cycle progression. Cumulative histogram displaying the percentage of cells in the G1 phase of the cell cycle (%G1), for homozygous diploid deletion strains. The bin width of the histogram is 1%, with each bin containing all the strains with values within the bin boundaries. The black line superimposed to this histogram is the normal distribution fit of the %G1 values of the reference wild type strain. Bins with values >2 sd from the mean of the wild type distribution are in red ("Low G1" group) and green ("High G1" group).

A large number of gene deletions affect the G1 phase of the cell cycle. From all strains analyzed successfully (n=4, 342; Dataset C-1), 152 were in the "High G1" group, but only 16 were in the "Low G1" group. Hence, the majority of gene deletions that affect cell-cycle progression lead to a G1 delay (Fig. 2). We expect that additional gene deletions affect cell-cycle progression, but were not included in the "High G1" or "Low G1" groups, for at least two reasons: experimental error; and imposition of restrictive cutoffs (>41.57%G1 for the "High G1" group and <20.77%G1 for the "Low G1" group). An example of the latter is *whi5Δ* cells, which lack an inhibitor of START (20, 22). *whi5Δ* cells clearly had "Low G1" DNA content, with ~25% of cells in G1 (compared to

~31% for wild type cells), but that value was still within 2 sd of the WT mean (Fig. 2). To examine the issue of false negatives in more detail, we determined the timing of START in two strains, which were close to our cutoffs, but not included in the candidate lists. Each of these strains lacked a protein kinase of unknown function: Kns1p (74) (*kns1Δ* cells had a 27% G1 score), or Tda1p (86) (*tda1Δ* cells had a 39% G1 score).

DNA content measurements from asynchronous cultures only reflect the *relative* duration of the G1 phase compared to the rest of the cell-cycle phases. For example, a given deletion could increase the length of not only the G1 phase, but also subsequent phases. In that case, if the mitotic phases are disproportionately expanded compared to the G1 phase, that strain will display a "Low G1" DNA content, despite its lengthened G1 phase. To address this possibility, we obtained estimates of the *absolute* length of the G1 phase. The length of the G1 phase of a strain cultured in any given medium can be measured if one knows three parameters: i) the size of newborn cells ("birth" size). ii) the "critical size" these newborn daughter cells must attain to initiate cell division. iii) the rate ("growth rate") at which they grow from their birth size to their critical size. Values for each of these variables can be obtained in yeast studies. From cell size distributions of log-phase cultures obtained with a channelyzer, daughter "birth" size was defined as the maximum size of the smallest 10% of cells on the left side of the cell size distribution of each strain. Wild type, *kns1Δ* and *tda1Δ* cells had indistinguishable cell size distributions (Fig. A-2A), and the same birth size (~35 fl), in this medium (YPD-0.5% Dextrose). To obtain the "critical size" and "growth rate" of these strains, we examined highly synchronous, elutriated cultures (6, 7, 43). As a function of time, we

measured cell size and the percentage of budded cells (budding correlates with START completion). We found that there was no difference between wild type and *kns1Δ* cells (Fig. A-3). In contrast, *tda1Δ* cells delay START, not because they have altered critical size (Fig. A-3B), but because they reach that size more slowly than do wild type cells (Fig. A-3A). Hence, our cutoffs exclude some gene deletions with cell-cycle effects, such as *whi5Δ* or *tda1Δ* cells. Therefore, despite the large number of gene deletions we identified to alter cell-cycle progression significantly, we have likely underestimated that number.

Most gene deletions that affect cell-cycle progression do not alter cell size. We found that reduced fitness (35) correlates with altered cell-cycle progression to some degree (Fig. 3). Nevertheless, many gene deletions affect cell-cycle progression, without affecting fitness. Cells that spend relatively more time in a particular cell-cycle phase may not display reduced fitness because reciprocal, compensatory changes in the duration of other cell-cycle phases may result in no net change in total generation time. Several known cell-cycle mutants behave in this manner (e.g., *whi5* cells (52)).

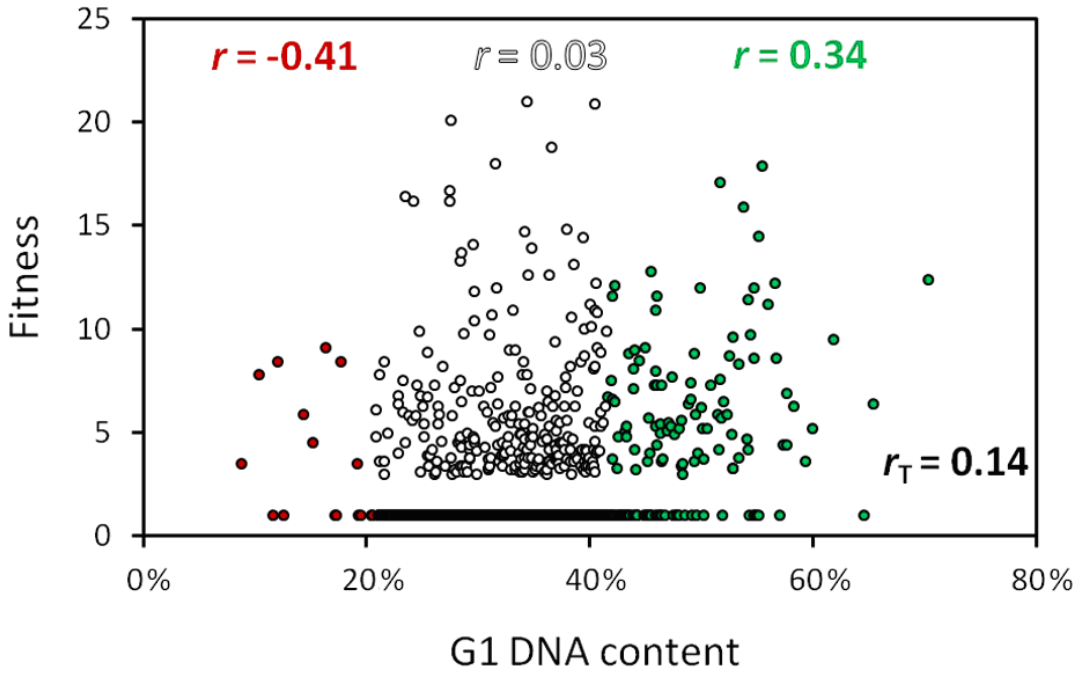

FIG 3 Decreased fitness correlates with altered cell-cycle progression. The y-axis shows the fitness values of Giaever et al (35). Higher values indicate reduced fitness. The cutoff for reduced fitness was about <85% of the wild type in that study (35). Thus, strains with possible small reductions in fitness have been assigned a "WT-like" fitness score of 1. Giaever et al (35) evaluated fitness of the same strains we used, during growth in rich (YPD-2%Dextrose) liquid media, allowing for a direct comparison with our dataset. We used the non-parametric Spearman test to obtain the correlation (r) values we show. The correlation coefficient for all the strains (r_T) is shown at the bottom right of the graph. We colored the r values for the sub-groups as in Fig. 2. For every gene we included in this analysis, the values we used in this correlation are shown in Dataset C-1.

We then compared %G1 values against cell size (52, 120). We expected a strong negative correlation between cell size and the fraction of cells with unreplicated genome, since cells grow larger as they advance in the cell cycle. Remarkably, however, there was only a very weak, negative correlation between %G1 and cell size (r=-0.14, Fig. 4 and A-4). Most of the deletion strains displaying a longer G1 (the "High G1" group) did not have altered cell size (Fig. 4, strains between the dashed lines; and Fig. A-4). Conversely, many strains classified as size mutants (52, 120) did not have significantly

altered DNA content (Fig. 4, open circles outside the dashed lines, and Fig. A-4). These data show that changes in cell size are neither necessary nor sufficient for altered cell-cycle progression. In the Discussion, we describe the implications of these results in the context of previous attempts to identify cell-cycle regulators based on cell size changes.

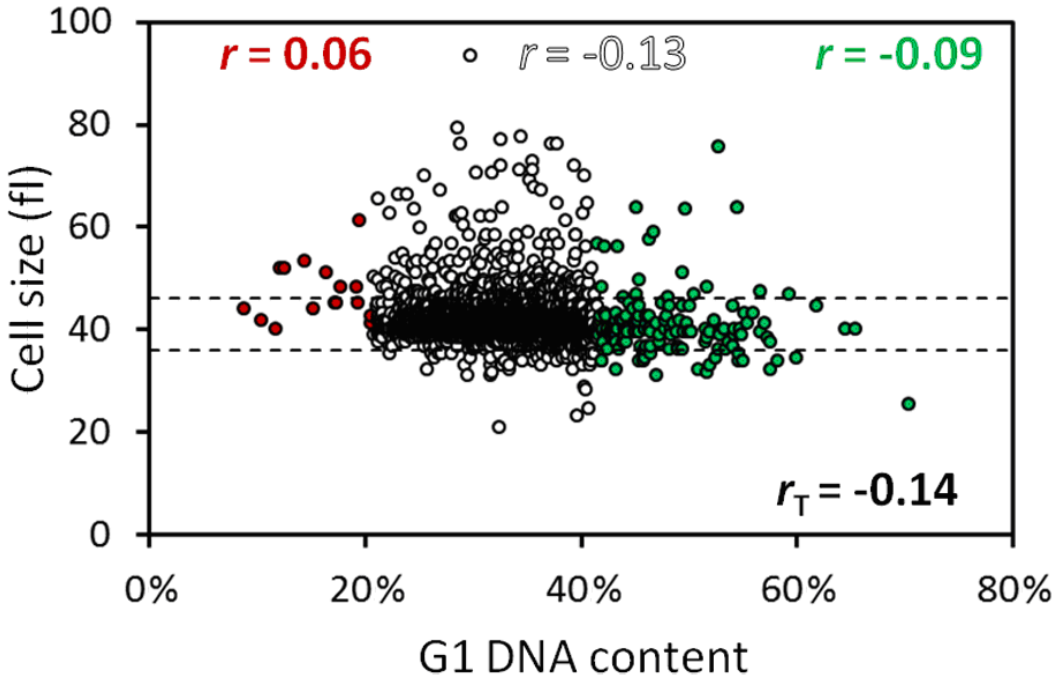

FIG 4 Cell size correlates poorly with DNA content. We plotted the %G1 (x-axis) from all the deletion strains we examined against the haploid median cell size (in fl, y-axis) data of Jorgensen et al (52). The dashed lines indicate the cutoffs used to define *whi* (bottom) and *lge* (top) mutants in that study. We calculated and displayed the *r* values as in Fig. 3. For every gene we included in this analysis, the values we used in this correlation are shown in Dataset C-1.

Along with DNA content, we also analyzed the forward scatter (FSC) from the same flow cytometry experiments. FSC values often serve as a proxy for cell size, especially in animal model systems (4, 59). An overall negative correlation between FSC values and %G1 was present (r=-0.26, Fig. A-5). However, we noticed some

discrepancies. For example, in the "High G1" group %G1 correlated to some extent with FSC (r=-0.31), but much less with actual cell size (r=-0.09, Fig. 4). We then correlated FSC values to cell size. Surprisingly, for the majority of strains, FSC values do not correlate well with published (52, 120) cell size values (Fig. A-6). These data generally suggest that inferring cell size phenotypes from FSC measurements is problematic.

We next asked if there is a correspondence between genes that affect cell division when over-expressed, with genes required for normal cell-cycle progression. We compared our data set to the genes identified in a systematic over-expression screen, which also relied on DNA content changes (70). In only one case did over-expression of a non-essential gene have the reciprocal effect of its deletion (*NIP100*, encoding the large subunit of dynactin; Table B-2). On the other hand, about half of the deletion strains with a low budding index (119) also had a high %G1 (Table B-3). This is reasonable, since budding correlates with START completion (83).

Deletion of genes involved in ribosomal biogenesis and protein synthesis delay START. The "Low G1" group is enriched for "cell cycle" gene ontologies (Table B-4). We point out the *sic1Δ* strain, which was the 2nd-highest ranked strain of the group. Sic1p is a Cdk inhibitor of Clb/Cdk complexes, which is destroyed before cells initiate DNA replication (8). Cells lacking Sic1p are not small size mutants (52, 120), and Sic1p was identified biochemically, as a Cdk-associated protein (68). The "High G1" group is enriched for genes involved in "cytoplasmic translation" and "ribosome biogenesis"

(Table B-5). This is consistent with protein synthesis and ribosome biogenesis being required for the timely completion of START (2, 42, 69, 80, 107).

In our analyses, we considered a high G1 DNA content and a lengthened G1 phase indicative of *delayed* START. We noticed that some of the genes involved in ribosome biogenesis and protein synthesis that we found with a "High G1" DNA content, were also classified by others as small size mutants with *accelerated* START (52, 53). For example, *sfp1Δ* cells, which lack a transcription factor important for ribosome biogenesis (31, 52, 67), was the 2nd highest-ranked gene deletion in our "High G1" group (see Fig. A-1 and Dataset C-1). Yet, although the high G1 DNA content of *sfp1Δ* cells was noted (52), because of the small size of *sfp1Δ* cells, others concluded that START was accelerated in these cells (53).

To resolve these discrepancies, we decided to examine transit through G1 and START completion in *sfp1Δ* cells. We did these experiments in YPD medium with 2% Dextrose, because Jorgensen et al used the same medium in a similar analysis of *sfp1Δ* cells (53). Under these conditions, wild type cells have a "birth" size of 42.12±1.23 fl (n=3) and a "critical" size of 61.53±0.64 fl (n=8). We found that *sfp1Δ* cells had dramatically reduced "birth" (16.04±0.62 fl, n=3, P=6.9x10^{-5} based on a *t* test, see Fig. A-2B) and "critical" (39.23±0.53 fl, n=6, P=2.1x10^{-10}, Fig. 5C, A-7) sizes, and "growth rate" (Fig. 5A, 5B, A-7). We calculated the "growth rate" differences between wild type and *sfp1Δ* cells in two different ways (see Materials and Methods), assuming that growth is exponential or linear. If growth is exponential, then *sfp1Δ* cells grow at ~50% the rate of wild type cells (Fig. 5B, A-7). If growth is linear, then *sfp1Δ* cells grow at ~30% the

rate of wild type cells (Fig. 5A, A-7). For all other comparisons of "growth rates" between different strains that we present in this study, we obtain similar results, regardless of whether we plot size increases in an exponential or a linear manner, because the overall size of those strains is similar to wild type. However, given the strong cell-size phenotype of *sfp1Δ* cells, and since exponential growth incorporates cell size differences (i.e., smaller cells grow more slowly than large cells), the growth rate decrease of *sfp1Δ* cells compared to wild type appears somewhat less if one assumes exponential increase in size. Nonetheless, regardless of whether growth is linear or exponential, it is clear that the G1 phase of *sfp1Δ* cells is substantially expanded (~4-fold, see Materials and Methods for calculations). Cells lacking Sfp1p have a long G1 because they are born sufficiently small and grow sufficiently slowly to overcompensate for any theoretical shortening of the phase due to small critical size. Therefore, their small size notwithstanding, we conclude that START is severely delayed in *sfp1Δ* cells. We expand on this interpretation further in the Discussion.

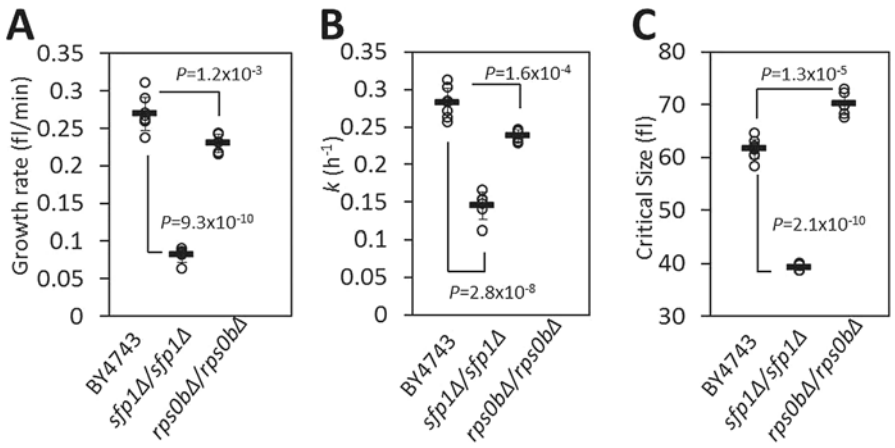

FIG 5 Deletion of genes involved in ribosome biogenesis delay START. (A) Rate of cell size increase (shown as growth rate, in fl/min) for the indicated strains was measured from synchronous elutriated cultures, in YPD-2% Dextrose medium. The average value for each strain was calculated assuming linear growth and is shown with a horizontal bar (± sd). Where indicated, the *P* values shown were calculated from two-tailed *t* tests. The data used to calculate these values are shown in Fig. A-7A. (B) The specific rate of cell size increase constant *k* (in h^{-1}) was measured from the same elutriation experiments shown in A, assuming exponential growth. The data used to calculate these values are shown in Fig. A-7B. (C) The critical cell size of the indicated strains (shown in fl), was measured from the same elutriation experiments shown in A and B (see also Fig. A-7C).

To probe the connection between ribosomes and START further, we next evaluated *rps0bΔ* cells, another mutant with small size (52), lacking one of the Rps0 variants of the 40S ribosome particle. Cells lacking *RPS0B* have a high G1 DNA content (54%, see Dataset C-1). We found that *rps0bΔ* cells have a reduced "birth" size (34.53±1.89 fl, n=3, *P*=0.007 based on a *t* test, see Fig. A-2B), an increased "critical" size (70.06±1.90 fl, Fig. 5C, A-7), and a slow "growth" rate (Fig. 5A, 5B, A-7). From these data, we conclude the following: i) since each of these changes alone would be sufficient to prolong G1, the combination of all three adequately explain the significant G1 delay of *rps0bΔ* cells, ii) "birth" size is not necessarily a predictor of "critical" size,

and vice versa, since the two values can be highly discordant, as in *rps0bΔ* cells, and iii) DNA content measurements incorporate contributions of all these variables, including growth rate, successfully identifying the long G1 and delayed START of *rps0bΔ* cells.

Next, we examined if there are any patterns in the requirement of ribosomal proteins for the timely completion of START. Intriguingly, although deletion of ribosomal protein subunits delayed START in general, the effect was much greater upon loss of 40S ribosomal proteins (RPSs), compared to the 60S subunits (RPLs; Fig. 6A). In contrast, loss of RPSs or RPLs had similar effects on fitness (Fig. 6B) and cell size (Fig. 6C).

Networks of genes affecting cell-cycle progression. Factors with related biological functions show genetic interactions more often than expected by chance (104). We queried the BioGRID database (100), for interactions among the genes we identified. Most of the factors of the "Low G1" group have multiple interactions with each other (Fig. 7). In the "High G1" dataset, we also noted several highly connected factors (Fig. 8), including the SR protein kinase Sky1p, similar to human SRPK1, which is involved in regulating proteins involved in mRNA metabolism. A group of genes in the "High G1" dataset that does not appear to interact with the rest of the group is composed of subunits of the vacuolar ATPase (Fig. 8, bottom). Finally, we also noted an interaction between a metabolic enzyme, Cys4p, and the Cdk Cdc28p (34).

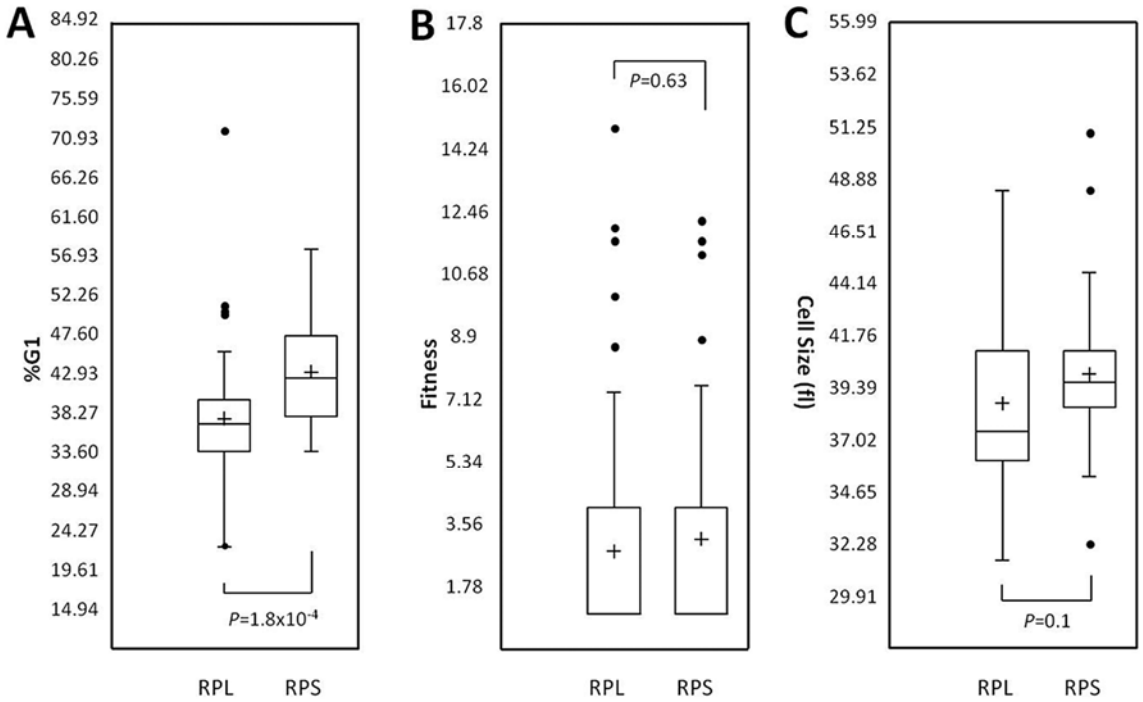

FIG 6 Phenotypes of ribosomal proteins. We grouped strains (n=53) that lack ribosomal proteins of the 60S subunit (RPL), against strains (n=43) that lack ribosomal proteins of the 40S subunit (RPS). We then compared the two groups based on the %G1 DNA content (this study, (A); fitness (data from Giaever et al (35), (B); or haploid median cell size (data from Jorgensen et al (52), (C)) The box plots were generated with Microsoft Excel. The box represents the middle 50% of the data range (from the 25th percentile to the 75th percentile). The band within the box is the median, while the cross shows the mean. The ends of the whiskers represent the lowest datum still within 1.5 of the interquartile range (IQR) of the lower quartile, and the highest datum still within 1.5 IQR of the upper quartile. Any data points not included within the whiskers are shown as outliers, displayed as filled circles. For the fitness data in B, the lower quartiles are not visible, because they are equal to 1 (i.e., most strains have fitness values similar to WT). The *P* values were calculated from *t* tests.

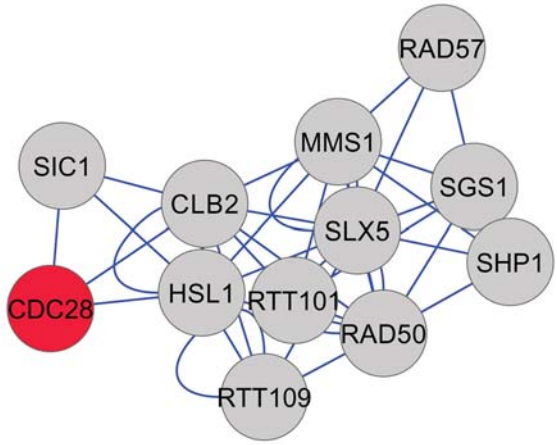

FIG 7 Network representation of the "Low G1" group. The interactions shown are from the gold-standard reference database BioGRID (100). The network was constructed with Cytoscape (98), and displayed using an unbiased, force-generated layout. Only the factors that showed interactions (physical or functional) are included. We also included the essential gene *CDC28* (shown in red), encoding the major yeast Cdk.

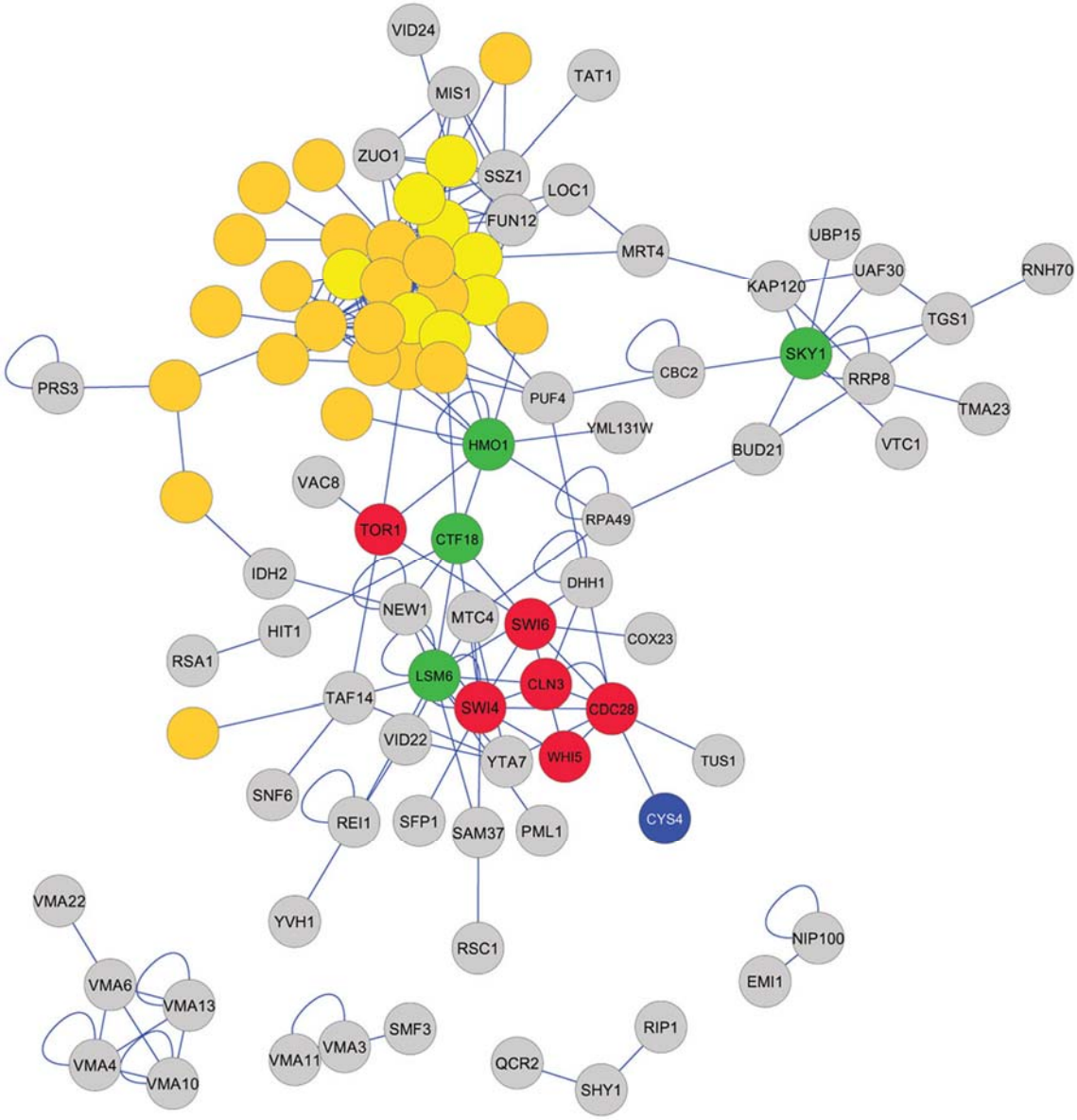

FIG 8 Interactions among the factors of the "High G1" group. The network of interactions was constructed and displayed as in Fig. 7. We also included factors with known roles at START (shown in red), which were not identified in our study. Among the G1 cyclins, we only included Cln3p, which is responsible for initiating the positive feedback loop of the large G1/S transcriptional program (25, 30, 96). The other G1 cyclins, Cln1p and Cln2p, are important for this feedback, once it is initiated by Cln3p, but they were not included in this network. 60S ribosomal proteins are in yellow, while 40S ribosomal proteins are in orange. The most highly connected factors among the ones we identified are in green, and Cys4p is in blue.

A non-catalytic function of Cys4p promotes START. *CYS4* encodes the yeast CBS. We focused on Cys4p because we had previously shown that cells with a hypermorphic *CYS4* allele accelerate START (6). Since the loss of Cys4p delays START (see Dataset C-1), we queried the effects of Cys4p over-expression on START. To measure the timing of START, we examined highly synchronous, elutriated cultures. All strains cells had indistinguishable cell size distributions (Fig. A-2C) and the same birth size (~14 fl, Fig. A-2C) in this medium (YPGal-3% Galactose). Consistent with Cys4p's metabolic role (6), we found that over-expression of Cys4p, but not of the catalytically inactive Cys4p-S289D variant (84), increased growth rate (Fig. 9A). Over-expression of Cys4p also reduced the critical size for START (Fig. 9B). Hence, wild type Cys4p accelerates START both by increasing growth rate, and by reducing critical size. Taking both of these variables into account, we conclude that over-expression of Cys4p shortens the length of the G1 phase by ~30% (see Materials and Methods for calculations). Remarkably, over-expression of Cys4p-S289D also decreased critical size (Fig. 9B, right). These results suggest that Cys4p promotes START in two ways: first, by promoting cell growth, which requires its catalytic activity, and second, by reducing critical size fully independently of catalytic activity.

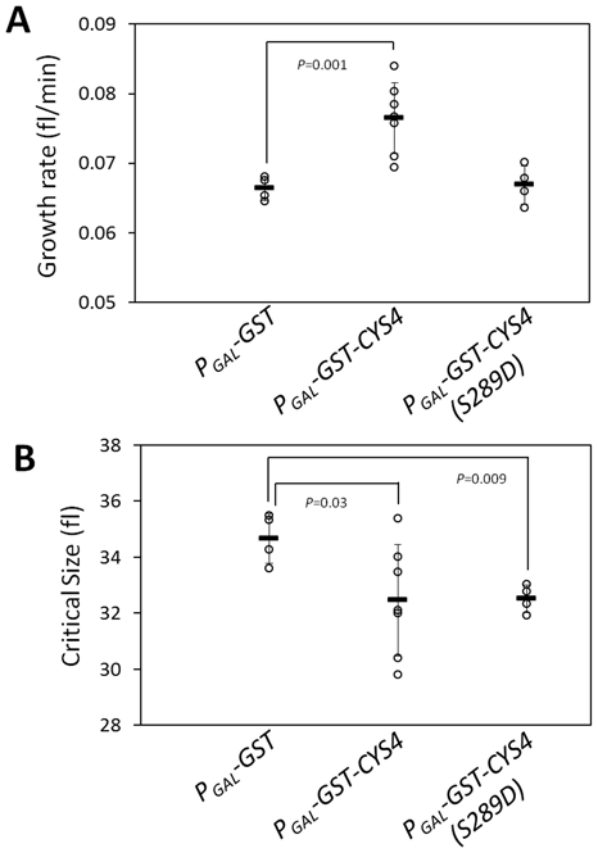

FIG 9 Cys4p advances START both by promoting cell growth and by a separate function, which does not require CBS's catalytic activity. (A) Rate of cell size increase (shown as growth rate, in fl/min) for the indicated strains was measured assuming linear growth from synchronous elutriated cultures in media that contain galactose and induce expression of the P_{GAL} alleles (see Materials and Methods). The average value for each strain is shown with a horizontal bar (± sd). Where indicated, the *P* values shown were calculated from two-tailed *t* tests. The data used to calculate the values shown in A and B are in Fig. A-8. (B) The critical cell size of the indicated strains (shown in fl), was measured from the same elutriation experiments shown in A (see also Fig. A-9). The analogous experiments in non-inducing, glucose containing, medium are shown in Fig. A-9.

Yeast lacking *CYS4* can be viable if supplemented with cysteine (18). In the standard S288c strain background we used here, *cys4Δ* cells proliferate more slowly than wild type (~2 to 3-fold), even in rich media (35). In humans, patients with CBS deficiency have high levels of homocysteine. These patients have brain, skeletal and vascular abnormalities (33). There are more than 130 pathogenic CBS mutations, but not

all of them affect the activity of CBS (92). *Cbs*$^{-/-}$ mice have high levels of homocysteine (>200μM) and die within weeks after birth (112). In *Cbs*$^{-/-}$ mice, cells critical for the development of the cerebellum cannot proliferate (27). Introducing human *CBS* alleles that encode inactive enzymes did not reduce the homocysteine levels of these mice, but these transgenes *did* rescue the neonatal lethality of *Cbs*$^{-/-}$ mice (111). Thus, in animals, CBS must have essential, non-catalytic roles. Because of these observations, we asked if the catalytic role of Cys4p is separable from the proliferative defects associated with loss of Cys4p in yeast. We generated strains that express Cys4p-S289D at endogenous levels (Fig. 10A, lanes 3 & 4). These strains are cysteine auxotrophs (Fig. 10B, middle panel), consistent with their lack of Cys4p catalytic activity. However, when cysteine is present, they proliferate much better than strains that lack Cys4p altogether (Fig. 10B, lower panel). These results are in remarkable agreement with the data in mice: loss of CBS leads to proliferative and metabolic defects (homocysteinuria in mice, cysteine auxotrophy in yeast). In both organisms, inactive CBS does not suppress the metabolic defects, but it suppresses the proliferative defects.

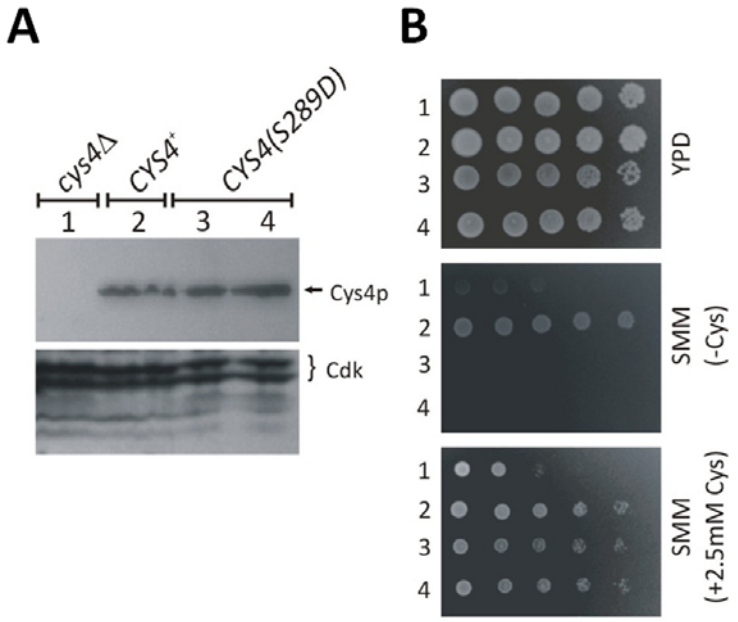

FIG 10 Cys4p has a vital, non-catalytic role in cell proliferation. (A) Immunoblots showing the levels of Cys4p in the indicated strains, detected with an antibody against human CBS. We probed the same blot with an antibody against yeast Cdc28p, to indicate loading. (B) Growth of the same strains on rich (YPD) and synthetic minimal media (SMM). We added cysteine (at 2.5 mM), to the SMM plate at the bottom. All strains were spotted on plates at 5-fold serial dilutions from liquid cultures, starting at ~5, 000 cells.

2.2 Atypical or unquantifiable cytometry profiles

As detailed above, we interrogated the yeast deletion collection of nonessential genes for altered DNA content by flow cytometry (45). Most strains displayed DNA content histograms with well-defined peaks, corresponding to cells with unreplicated (G1 phase of the cell cycle), or fully replicated genome (in the G2 or M phases of the cell cycle). Well-defined DNA content profiles allow for automated quantification of the percentage of cells in different phases of the cell cycle. However, we could not include in that analysis deletion strains with complex, unquantifiable DNA content profiles. These DNA content profiles could arise from abnormal DNA replication, chromosome

segregation, cytokinesis or cell separation. Hence, information from DNA content analysis will be helpful to efforts aiming to understand these important cellular processes. Here, we present a survey of all the deletion strains that reproducibly displayed complex DNA content profiles. To our knowledge, such an analysis has not been reported previously.

We visually examined and manually curated each DNA content profile. We identified deletion strains that in at least two independent experiments reproducibly displayed complex DNA content profiles. In arranging the DNA content histograms, we took into account not only the overall appearance of each profile, but also the mean fluorescence intensity in each case (mean FL-A values, see Fig. 11). For example, cells lacking *HFI1*, encoding a protein adaptor of the SAGA histone acetyltransferase-coactivator complex (3), had a DNA content profile with some well-defined peaks. However, the profile was shifted overall, to the left along the x-axis, with low mean fluorescence intensity (Fig. 11). The left-most peak may represent *hfi1Δ* cells with sub-G1 DNA content. Alternatively, the overall shift to the left may result from lower overall DNA staining, perhaps due to unusual chromatin structure of *hfi1Δ* cells.

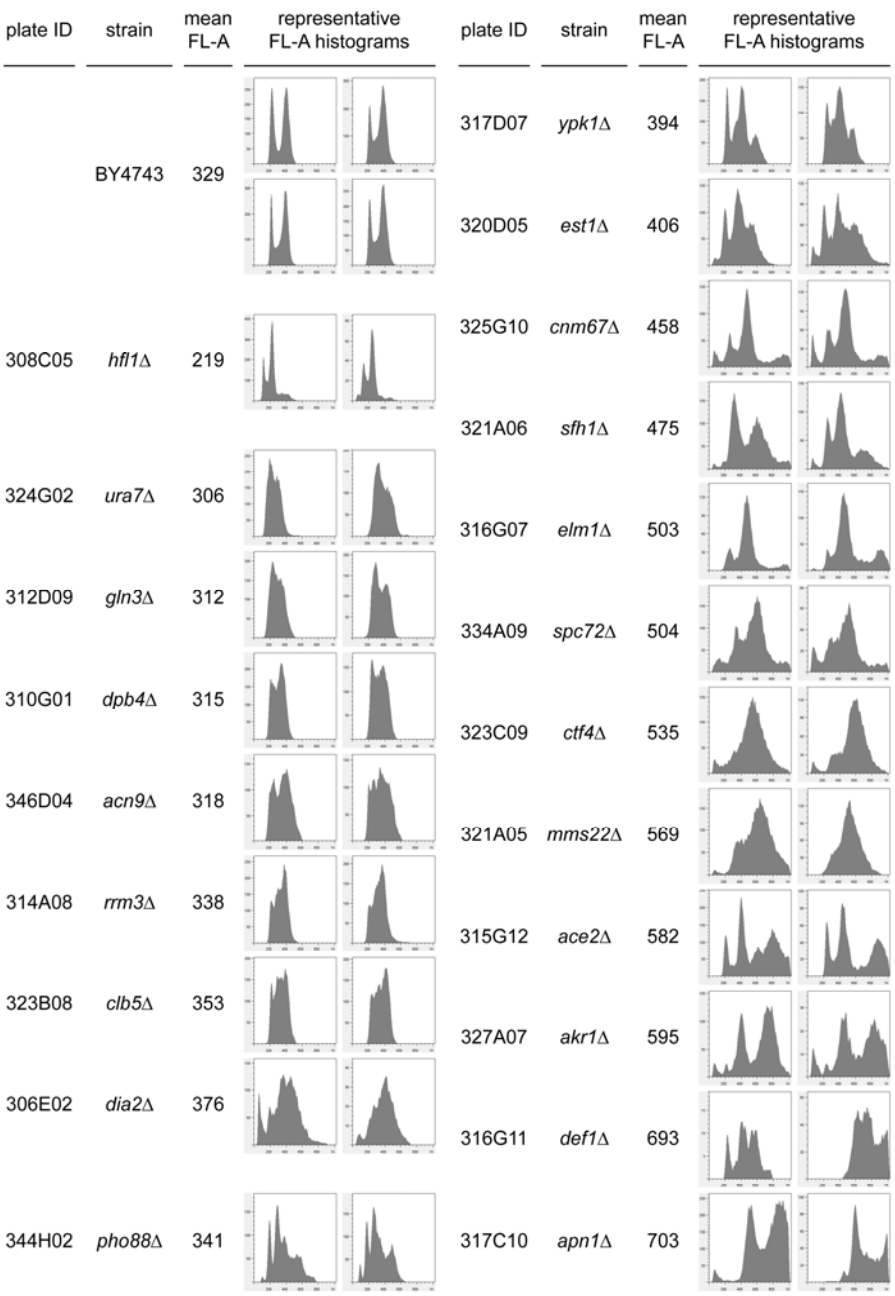

FIG 11 Homozygous diploid deletion strains with complex DNA content. BY4743 is the wild type, diploid reference strain. For all other strains, DNA content histograms from two independent experiments are shown in each case. Fluorescence is plotted on the x-axis, while the number of cells analyzed is on the y-axis. The plate ID number refers to the position of these strains in 96-well plates, as they were supplied from Open Biosystems. The mean fluorescence values (FL-A) are shown for each strain. The profiles for *clb5Δ* and *elm1Δ* cells have also been shown in an earlier study. All methods and information on data acquisition have been described elsewhere.

The next group of gene deletions (*ura7Δ, gln3Δ, dpb4Δ, acn9Δ, rrm3Δ, clb5Δ, dia2Δ*; Fig. 11) has a DNA content profile suggestive of abnormalities during DNA replication. Indeed, several of the corresponding gene products have well established roles during DNA replication. Dpb4p is a subunit of DNA polymerase ε (71). Rrm3p is a DNA helicase involved in DNA replication (66). Clb5p is an S-phase cyclin (8), while Dia2p is a protein that binds to origins of DNA replication (60). Loss of the transcription factor Gln3p has been reported to lead to a DNA content profile consistent with cells accumulating in the S-phase of the cell cycle (114), probably because Gln3p affects expression of ribonucleotide reductase (64). Similarly, loss of Ura7p, the major subunit of CTP synthase involved in pyrimidine synthesis and maintenance of nucleotide pools (73), may explain the accumulation of cells during the S-phase of the cell cycle. However, we also found in the same group cells lacking Acn9p, a protein reported residing in mitochondria (23). Although Acn9p, which is conserved in humans, has putative metabolic roles (23), its exact molecular function is unknown. Our data suggest that Acn9p's function is critical for some aspect of DNA replication, directly or indirectly. We also found that cell lacking Pho88p, a putative membrane protein implicated in phosphate transport (117), have a DNA content profile with multiple peaks (shown at the bottom left of Fig. 11), which are somewhat better defined than in the rest of the deletion strains we mentioned above with a more typical "S-phase" DNA content profile.

Next, we identified a set of deletions strains in which a fraction of cells has DNA content higher than a fully replicated diploid genome. These DNA content profiles are

shown on the right of Fig. 11. The gene products deleted in these strains include several with known roles in cytokinesis or cell separation. Elm1p is a protein kinase involved in cytokinesis (11). Ace2p is a transcription factor important for the destruction of the septum after cytokinesis (89). Finally, Def1p, a chromatin-associated protein with roles in transcription elongation, also has been implicated in cytokinesis (51). Other gene products in this group have already been reported to function in chromosome maintenance and segregation. Ypk1p is a pleiotropic protein kinase with roles during progression through the G2 phase of the cell cycle (99). Est1p is a telomere homeostasis factor (121). Cnm67p is a spindle pole component (91). Sfh1p is a component of the RSC chromatin remodeling complex whose loss impairs progression through the G2/M transition of the cell cycle and it is required for normal ploidy (14). Spc72p is a component of γ-tubulin that binds spindle pole bodies (44). Ctf4p is required for sister chromatid cohesion (41). Mms22p is a subunit of an E3 ubiquitin ligase with roles in DNA replication and repair and chromosome segregation (108). Finally, Apn1p is a DNA repair endonuclease (9). Surprisingly, however, we also found that cells lacking Akr1p have DNA content higher than a fully replicated diploid genome (Fig. 11). Akr1p is a palmitoyl transferase (87), which to our knowledge has not been previously implicated in cytokinesis or chromosome maintenance.

In summary, for most of the deletion strains we examined here, their DNA content profiles validate and support the function(s) previously ascribed to the corresponding gene products during DNA replication and chromosome maintenance. Importantly, however, our DNA content analysis also suggests previously unrecognized

roles in these processes for some gene products. For example, our data support a role for Acn9p in DNA replication and for Akr1p in chromosome maintenance. Since these proteins are conserved in most eukaryotes, including humans, the results we present may be significant for human biology.

2.3 Drug treatment analysis

We used a commercially available panel of 640 FDA-approved drugs (see Materials and Methods). We monitored the effects of each drug on cell-cycle progression by measuring the DNA content of the cells by flow cytometry (38) (see Fig. 12, and Materials and Methods). We did not quantify complex profiles (see Fig. 13), and we excluded the drug treatments that caused them from further analyses. At the beginning and end of most batches of samples, we measured the reference sample (a yeast strain that lacks the multidrug transporters Pdr5p and Snq2p, mock-treated with DMSO; see Materials and Methods), which was cultured and processed along with the cultures that were treated with drugs. We evaluated each drug in at least two independent experiments. We deposited all raw flow cytometry data in a public database (see Dataset C-2, and Materials and Methods).

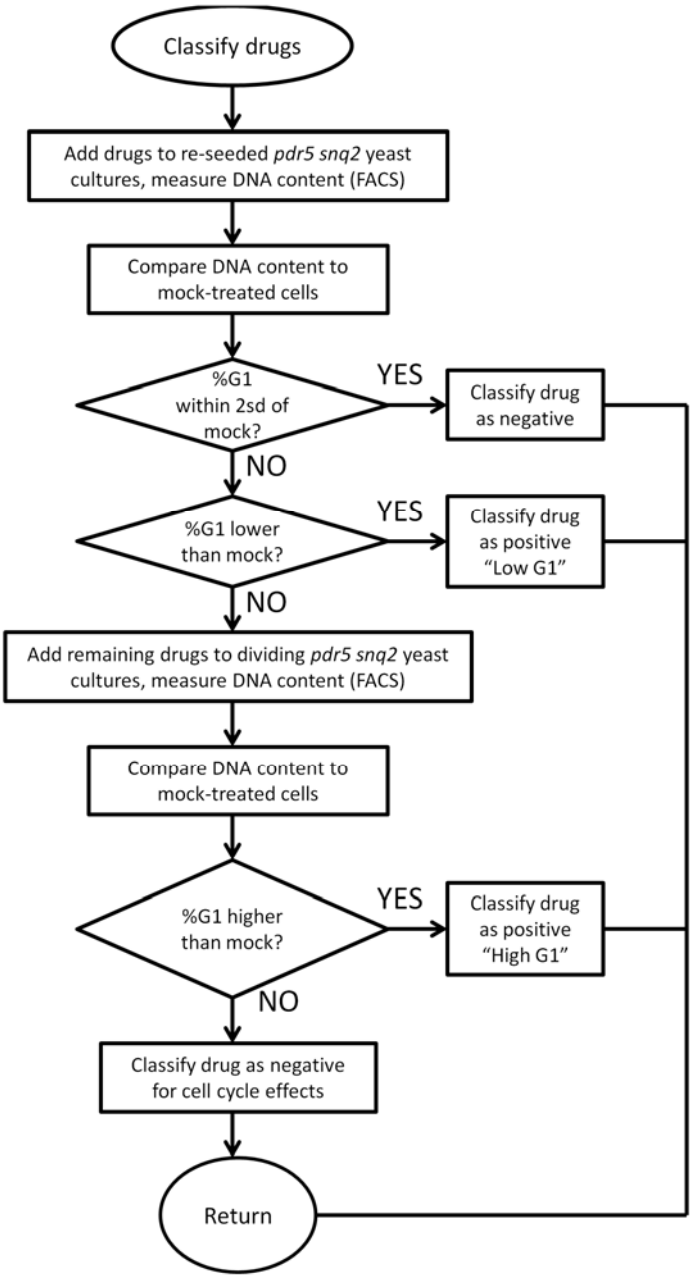

FIG 12 Decision flow-chart diagram of our primary analysis. This diagram summarizes our DNA content measurements using the *pdr5Δ, snq2Δ* strain. See text for details.

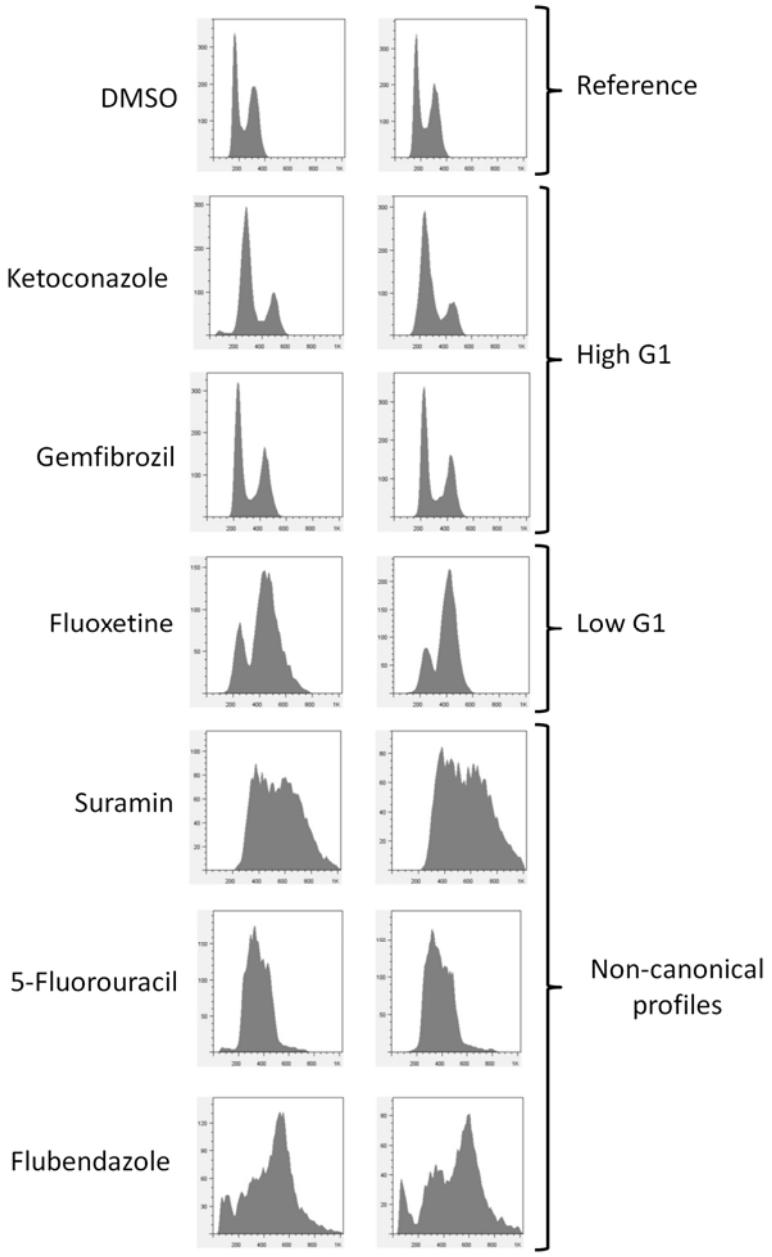

FIG 13 Representative DNA content histograms. Independent experiments of the indicated samples are shown in each case. Fluorescence is plotted on the x-axis, while the number of cells analyzed is on the y-axis. Reference samples were treated with DMSO, shown at the top. Examples of "High G1" profiles include cells treated with ketoconazole or gemfibrozil, while cells treated with fluoxetine give rise to a "Low G1" DNA content profile. At the bottom, we show a few examples of complex DNA content histograms that were unquantifiable. These include profiles of cells treated with suramin and 5-fluorouracil (antineoplastic agents), and flubendazole (a microtubule blocker used as anti-nematodal).

To identify drugs that altered the cell cycle, we compared the frequency distribution of cultures treated with drugs against a normal distribution fit of the reference (n=82) samples (Fig. 14A). Samples that had a %G1 greater or less than two standard deviations from the mean of the reference sample distribution were considered to differ significantly from the mock-treated samples (Fig. 12 and 14A). Drugs that led to an increase (%G1>60.00%) in the percentage of cells with unreplicated DNA formed the "High G1" group, while others led to a mitotic delay and a "Low G1" (%G1<38.76) DNA content (see Fig. 14A, and Dataset C-2). In this initial screen, we added the drugs to cultures diluted from an overnight stationary phase culture, where most cells would be in the G1 phase of the cell cycle (83). Hence, drugs in samples with a "High G1" DNA content may have arrested cell-cycle progression non-specifically. In that case, the high G1 DNA content reflected the state of the starting culture, and not cell-cycle effects of the drugs. To exclude such possibilities, we re-tested the "High G1" drugs by adding them to actively dividing cells (see Fig. 12). Overall, from this primary analysis we identified 27 compounds that interfered with progression in the G1 phase of the cell cycle, before initiation of DNA replication, resulting in a "High G1" DNA content (see Table B-6). Another 12 drugs affected mitotic progression, resulting in a "Low G1" DNA content (see Table B-7).

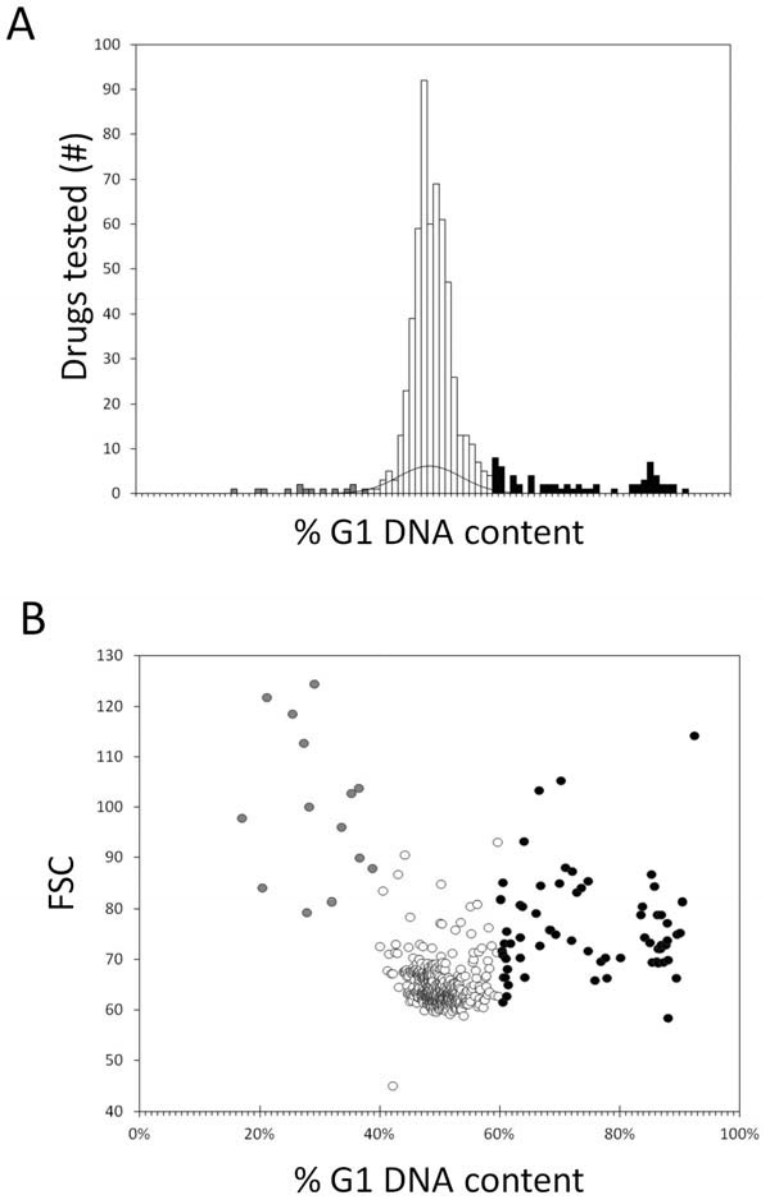

FIG 14 DNA content analysis identifies drug effects on cell-cycle progression. (A) Cumulative histogram displaying the percentage of cells in the G1 phase of the cell cycle (%G1), for cells treated with a panel of FDA-approved drugs. The bin width of the histogram is 1%, with each bin containing all the drugs with values within the bin boundaries. The black line superimposed to this histogram is the normal distribution fit of the %G1 values of the reference sample. Bins with values >2 sd from the mean of the wild type distribution are in grey ("Low G1" group) and black ("High G1" group). (B) From all the samples we analyzed by flow cytometry, the %G1 is on the x-axis, and the forward angle scattering (FSC) values on the y-axis. We colored the data points of the sub-groups as in A.

Along with DNA content, we also analyzed the forward scatter (FSC) from the same flow cytometry experiments (see Fig. 14B). FSC values often serve as a proxy for cell size, but they are also affected by cell shape and intracellular composition (56). We noticed that most drugs in the "Low G1" group had elevated FSC values compared to the group with no cell-cycle effects (Fig. 14B). This is consistent with the notion that mitotic delay leads to an increase of cell size. It should also be noted that yeast cells in mitotic phases of the cell cycle are budded (83). Hence, their irregular shape may also contribute to an increase in FSC values. An increase of FSC values was also evident for a significant fraction, but not all, of drugs in the "High G1" group (Fig. 14B).

We are not aware of other systematic studies of drug effects on cell-cycle progression measured by DNA content analyses. Our results reveal that several drugs currently and commonly used for human therapy have specific effects on the eukaryotic cell cycle. The higher number of drugs that interfered with G1 progression likely reflects the fact that cells commit to initiation of cell division in the G1 phase (50, 76, 83). Among the "High G1" group, we noted antifungals that inhibit biosynthesis of ergosterol, a component of fungal membranes (77), and rapamycin, a potent inhibitor of the TOR pathway known to block G1 progression (1). Overall, however, there was a diverse range of compounds in the "High G1" group (see Table B-6). Although most drugs in the "Low G1" group have well established mitotic roles (see Table B-7), we noted that the highest-ranked drug from this group was fluoxetine (brand name Prozac). To our knowledge, this is the first time that such strong cell-cycle effects have been reported for fluoxetine.

Since we did our primary analysis in a sensitized *pdr5Δ*, *snq2Δ* yeast strain, we then tested the drugs that led to the "High G1" and "Low G1" groups against the $PDR5^{+}$, $SNQ2^{+}$ wild type reference strain BY4741. We found that several drugs were not effective in this case. For example, lovastatin, which leads to a G1 arrest in mammalian cells (57), had no effect in $PDR5^{+}$, $SNQ2^{+}$ yeast cells (see Table B-6). This is consistent with an earlier report that yeast cells are sensitive to lovastatin in a *pdr5Δ* -dependent manner (32). Nonetheless, about half of the drugs in both groups remained effective in cells with intact multidrug transporters (see Tables B-6 and B-7).

Among drugs that led to a "High G1" DNA content, we further examined the cell-cycle effects of the potent antilipemic gemfibrozil (88), a Peroxisome Proliferator-Activated Receptor α (PPARα) agonist. To our knowledge, a G1 cell-cycle role for gemfibrozil has not been reported, in any system. The High G1 DNA content could result from roles specific to G1 progression, or manifest in G1 as a "carryover" from roles in other cell-cycle phases. To distinguish between these two possibilities, we added gemfibrozil to highly synchronous newborn G1 cells that we obtained by centrifugal elutriation (6, 7).

As a function of time, we then measured cell size and the percentage of budded cells (budding correlates with initiation of DNA replication in yeast (83)). This allowed us to measure the length of the G1 phase accurately, by calculating two parameters: i) the "critical size" these newborn daughter cells must attain to initiate cell division; ii) the rate ("growth rate") at which they grow to their critical size. DMSO-treated cells had a critical size of 63.2±2.4 fl and a specific growth rate constant k=0.328±0.008 h^{-1} (Fig.

15). Rapamycin markedly prolonged the G1 phase, in part because cells had to reach a substantially larger critical size (79.4±1.2 fl) before they could initiate DNA replication (Fig. 15A). Rapamycin-treated cells also grew very slowly (k=0.104±0.004 h^{-1}, Fig. 15B), although this effect was evident ~1 h after addition of the drug (Fig. A-10). We found that cells treated with gemfibrozil delayed initiation of DNA replication, not because they had altered critical size (65.4±0.6 fl, Fig. 15A), but because they reached that size more slowly than did cells treated with DMSO (k=0.287±0.07 h^{-1}, P=0.005, Fig. 15B). In addition, from the cell size distributions of asynchronously dividing cells, we obtained the "birth size" of newborn cells (see Materials and Methods). While DMSO-treated cells had a "birth size" of 40.3±2.7 fl under these growth conditions, gemfibrozil-treated newborn cells were significantly smaller (30.1±4.7 fl, P=0.04, Fig. 15C). Taken together, these data show that the smaller "birth size" and slower "growth rate" of cells treated with gemfibrozil lengthen the G1 phase.

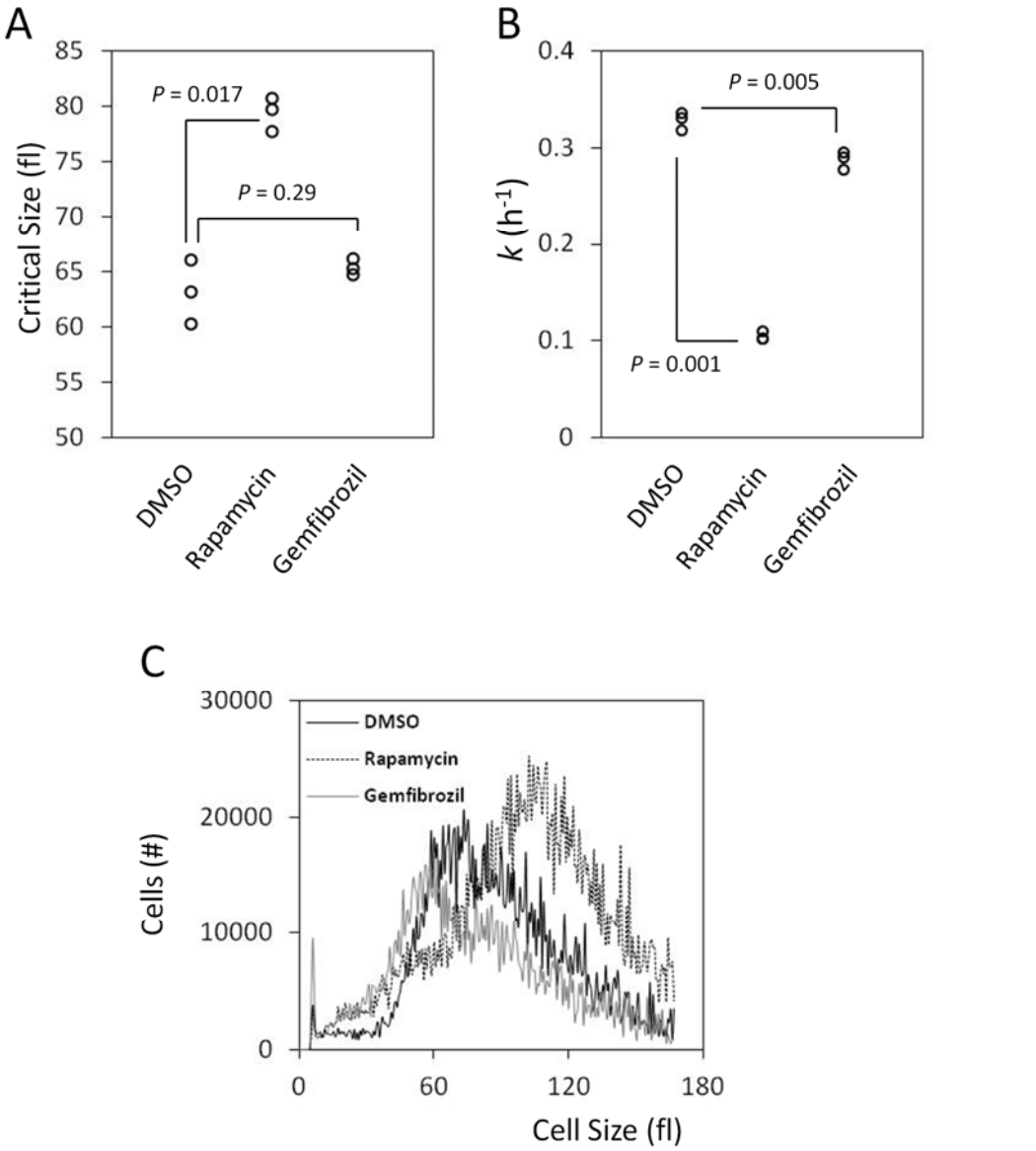

FIG 15 Gemfibrozil delays initiation of DNA replication. (A) The critical cell size (shown in fl) of diploid BY4743 cells treated with DMSO, rapamycin (0.1 μg/ml) or gemfibrozil (50 μg/ml), was measured from synchronous elutriated cultures, in YPD medium. The data points shown were from three independent experiments in each case. The *P* values shown were calculated from paired, two-tailed *t* tests, assuming unequal variance. The data used to calculate these parameters are shown in Fig. A-10. (B) The specific rate of cell size increase constant *k* (in h^{-1}) was measured from the same elutriation experiments shown in a, assuming exponential growth. The data used to calculate these parameters are shown in Fig. A-10. (C) The cell size distributions of the indicated cell populations, proliferating asynchronously in YPD medium, were measured using a channelyzer (see Materials and Methods, and (45)). Cell numbers are plotted on the y-axis and cell size (in fl) on the x-axis. Daughter "birth" size was defined as the maximum size of the smallest 10% of cells on the left side of the cell size distribution of each sample (45).

Next, we focused on the effects of gemfibrozil and fluoxetine on overall cell proliferation rates. We tested these drugs alone and in combination, at several doses (Fig. 16A). We found that gemfibrozil did not significantly affect overall cell proliferation at the doses tested (Fig. 16). Hence, the prolongation of the G1 phase by gemfibrozil is likely accompanied by compensatory shortening of subsequent cell-cycle phases, resulting in similar overall generation time. On the other hand, fluoxetine arrested proliferation of yeast cells at 200 μM (Fig. 16A, first green bar to the left; and Table B-8, bottom left cell). To our knowledge, the near complete inhibition of yeast cell proliferation by fluoxetine has not been reported. Remarkably, however, addition of gemfibrozil even at a 4-fold less molar concentration fully suppressed the inhibitory effects of fluoxetine (see Fig. 16A, compare the left green bar to the other green bars; and Table B-8, last row).

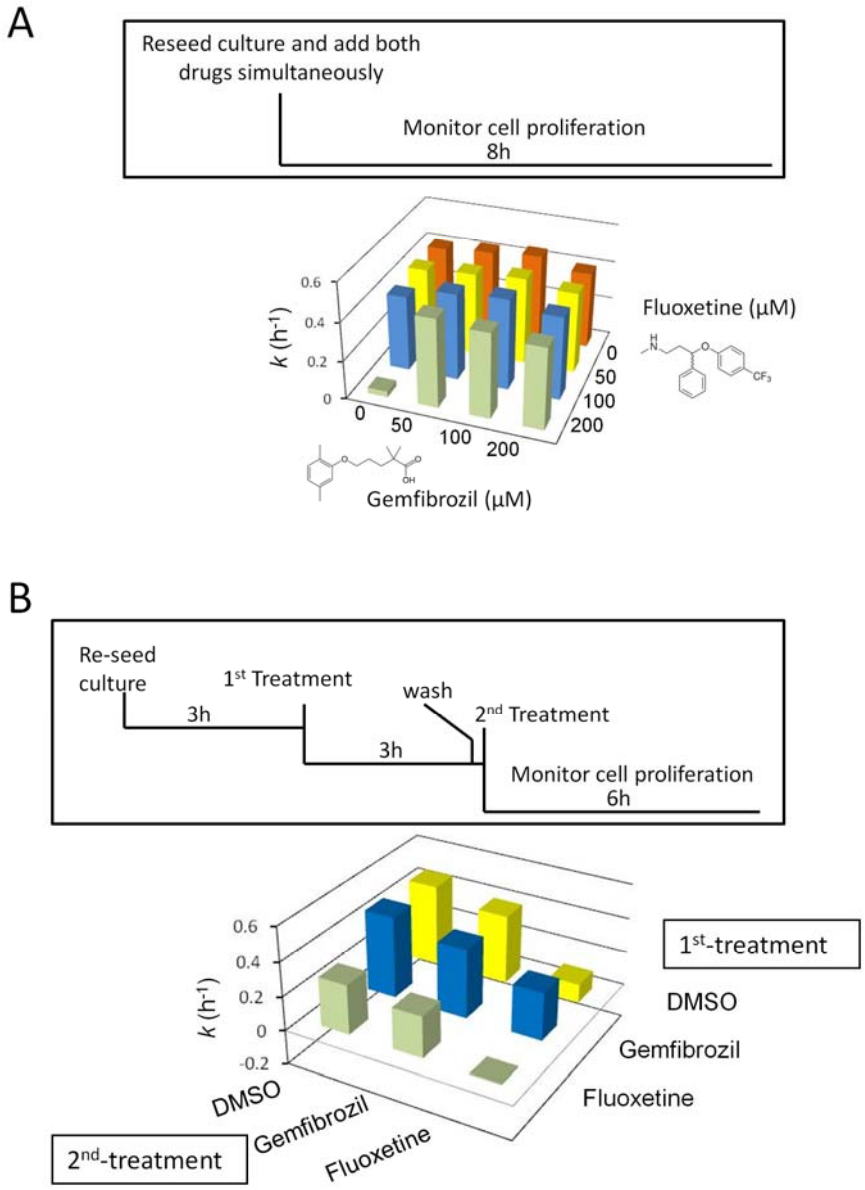

FIG 16 A novel interaction between gemfibrozil and fluoxetine. (A) Fluoxetine strongly inhibits yeast cell proliferation, but it is suppressed by gemfibrozil. We added to freshly reseeded wild type haploid yeast (BY4741) cells DMSO, fluoxetine and gemfibrozil at the binary combinations and concentrations shown. We then monitored cell proliferation hourly, for 8 h (see Materials and Methods). The specific growth rate constant (*k*) for each combination is shown. The errors associated with these measurements are shown in Table B-7. (B) DMSO, fluoxetine and gemfibrozil were added to dividing cells at 200 μM in binary combinations, sequentially, in the order shown. Cell proliferation was monitored for 6 h as in a, with the specific growth rate constant (*k*) for each combination shown. Data from one representative experiment is shown. Suppressive effects of gemfibrozil on fluoxetine arising from order of addition were assessed by calculating growth rate constant (*k*) folds for gemfibrozil treatment over DMSO control for all experiments, initial treatment with gemfibrozil yielding a fold of 2.51 +/- 0.25, versus final treatment, 0.71 +/- 0.21, P-value = 0.000146.

We then added the two drugs not simultaneously, but in different order, removing the first drug before adding the second (Fig. 16B). We found that gemfibrozil suppressed fluoxetine's anti-proliferative effects only if added before (representative experiment in Fig. 16B, compare the blue and yellow bars on the right; and Table B-9, compare the top and middle cells in the 3rd column), but not after fluoxetine (Fig. 16B, compare the left and middle green bars; and Table B-9, compare the left and middle cells in the 3rd row). These results suggest that the suppressive interaction between gemfibrozil and fluoxetine is not due to extracellular interaction or competition for transport between the two drugs. Furthermore, the results from the order-of addition experiment suggest that gemfibrozil acts upstream, since it does not reverse fluoxetine's inhibition of cell proliferation. Instead, it appears that fluoxetine cannot inhibit cell proliferation in the context of gemfibrozil's prior action.

3. MATERIALS AND METHODS

3.1 Methods for genetic deletion analysis

Yeast protocols. *S. cerevisiae* strains used in this study are listed in Table B-1. Unless noted otherwise, we used standard yeast methods (55). To construct the P_{GAL} *-GST-CYS4* strain (Fig. 9, A-8, A-9), we started from a commercially available plasmid containing a P_{GAL} *-GST-CYS4* allele (Open Biosystems, cat#: YSC3869-95169400). However, this plasmid contained a frameshift mutation at nucleotide position 856 of the *CYS4* ORF, which we corrected. We then removed a BsrGI-SalI fragment, re-ligated the plasmid, and digested it with StuI. Finally, we integrated this linearized plasmid derivative containing the P_{GAL} *-GST-CYS4* allele at the *URA3* locus of W303-k699 (see Table B-1). We sequenced a similar plasmid supposed to carry a P_{GAL} *-GST-KIP3* allele (Open Biosystems, cat#: YSC3869-9518649), but we found that it only drives expression of GST, due to mutations downstream of the GST tag. We used this plasmid to construct the negative control P_{GAL}*-GST* strain (Fig. 9, A-8, A-9), as we described above. From the P_{GAL} *-GST-CYS4* plasmid we generated the P_{GAL}*-CYS4(S289D)* derivative, as follows: We used the P_{GAL} *-GST-CYS4* plasmid as a template in a PCR reaction with a forward primer encoding the S289D substitution, and a reverse primer complementary to sequences downstream of the *CYS4* ORF. The PCR fragment was then used to gap-repair the P_{GAL} *-GST-CYS4* plasmid, which was previously digested with BstEII. The resulting P_{GAL}*-CYS4(S289D)* plasmid was then used in the same way as above, to

construct the P_{GAL}-*CYS4(S289D)* strain (Fig. 9, A-8, A-9). All plasmids were sequenced and the resulting strains were verified for expression of the proteins of interest.

The *CYS4-13MYC* strain (Fig. 10) was made with a single-step PCR replacement (6). To make the *CYS4(S289D)-13MYC* strain (Fig. 10), we used genomic DNA of the *CYS4-13MYC* strain as a template in a PCR reaction with a forward primer encoding the S289D substitution, and a reverse primer complementary to sequences downstream of the *CYS4* ORF.

For DNA content measurements, strains were cultured standing at 30 °C in YPD (1% yeast extract, 2% peptone, 2% dextrose). Overnight cultures were diluted 1:500 into 1 ml fresh medium, cultured for 4-5 hrs, collected by centrifugation and fixed in 70% ethanol. To obtain size distributions from asynchronous cultures, overnight cultures of the strain and medium of interest were diluted 1:500 in fresh medium, and allowed to proliferate for 5-6 h, before we analyzed them. For synchronous cell-cycle analyses (6), strains were cultured and elutriated in YPD medium containing 0.5% dextrose (Fig. A-3, A-9), 2.0% dextrose (Fig. 5, S7), or YPGal (1% yeast extract, 2% peptone, 3% galactose; Fig. 9, A-8), as indicated.

Cell size determinations. Cell size was measured with a Beckman Z2 Channelyzer. For each sample we analyzed, we obtained size distributions from two different dilutions of cells. The average of the geometric mean of each size distribution was recorded. We used the Accucomp Beckman software package to obtain the statistics of each size distribution.

Measurements of critical size and growth rate from elutriated cultures. For isolation of early G1 daughter cells, cultures were grown in the medium indicated in each case at 30°C to a density of ~1-5x10^7 cells/ml, then fractionated with a Beckman JE-5.0 elutriator as described previously (7). Early fractions containing predominantly (>95%) small unbudded cells were collected by centrifugation, resuspended in the medium indicated in each case and incubated at 30°C. Every 20 min we monitored the percentage of budded cells and cell size. The "critical size" is the size at which 50% of the cells have budded in these experiments, and it was calculated as we described elsewhere (7). We calculated the rate of size increase, "growth rate" (in fl/min), assuming linear growth, as we described previously (7). To calculate "growth rate" assuming exponential growth, we plotted the natural log (ln) of cell size as a function of time (in h), see Fig. A-7B. We fit the data to a straight line using the regression function in Microsoft Excel. From the slope of the line, we obtained the specific rate of cell size increase constant (k, in h^{-1}). The average of all experiments for each strain was then calculated, along with the associated standard deviation. Since it sometimes took the cells longer to recover from the elutriation, we exclude this "lag" phase in our growth rate calculations. We derived growth rate data only from the linear portion of each experiment.

Estimates of the length of G1 were calculated as follows: Assuming linear growth, $G1_{(min)}$=("Critical Size"-"Birth Size")/"Growth Rate". Assuming exponential growth, $G1_{(h)}$=ln("Critical Size"/"Birth Size")/k.

Staining for DNA content analyses. Fixed cells were stored at 4 °C (overnight to 14 days). Cells were collected by centrifugation and stained overnight in 1 ml staining solution containing 50 mM sodium citrate pH 7.0, 0.25 mg/ml RNaseA, and 500 nM SYTOX Green (Molecular Probes, OR). Samples were stored at 4 °C overnight in opaque containers. Cell suspensions were sonicated briefly at the fixing and staining steps and immediately before flow cytometry.

Flow cytometry data acquisition, deposition and analysis. Stained cells were analyzed on a FACSCalibur (Becton Dickinson Immunocytometry Systems, CA) flow cytometer, using CellQuest (version 3.3; Becton Dickinson Immunocytometry Systems) acquisition software. Sytox Green fluorescence was collected through a 515/30-nm bandpass filter, and list mode data were acquired for 10, 000 cells defined by a dot plot of forward scatter (FSC) versus side scatter (SSC). Prior to each experiment, standard beads (Cyto-Cal Multifluor Intensity Beads, Thermo Scientific, CA) were used to calibrate the flow cytometer, and photomultiplier tube voltages were adjusted to place the highest intensity bead in the same channel (+/- 3). FACS files were archived at *Cytobank* (61). Automated quantification of the DNA content histograms was done with FlowJo 7.5 software. To exclude particulate non-yeast events, which had both very low FSC and low fluorescence (FL1/2-A), asymmetrical gates were fitted with the autogating tool. Gates were centered near FSC ~100 and FL1/2-A ~300 and contained all events of sufficient contiguity as defined by the default autogating parameters, on average ~91% of total. From the gated populations, we determined the mean and standard deviation of

the FSC parameter. Cell-cycle phase subpopulations were computed from the gated population using the Dean-Jett-Fox model without constraints. %G1 was defined as the area of the G1 model peak, divided by the combined areas of the G1 and G2/M peaks. Because the %G1 results represent a continuum, it was necessary to impose cutoffs in order to exclude model fits that did not accurately represent experimental data. This was assessed primarily by root mean square (RMS) error, which averaged 11.68 (+/- 2.80 standard deviation) across all included experiments. For this reason, we did not analyze experiments that yielded an initial model fit RMS >25, %G1<5%, or %G1>95% (since extremes in %G1 were often indicative of poor fit), except in a few cases where the model fit was visually inspected and/or manually constrained. Experiments for which the %G1 fell outside two standard deviations of the wild-type distribution were repeated additional times. Experimental data and correlations are provided in the searchable spreadsheet available as Dataset C-1. Raw data files can be freely accessed at Cytobank (www.cytobank.org) and are found in the public experiments "Yeast DNA Content Project – DELETION – INCLUDED", and "Yeast DNA Content Project – DELETION – EXCLUDED".

Statistical analysis. Non-parametric Spearman tests were done with the Analyze-it software package. In all other cases, statistical calculations were done with Microsoft Excel. Where indicated, *t* tests were 2-tailed, assuming unequal variance between data sets.

Yeast protein extracts. Protein extracts for immunoblots were made with the NaOH extraction method (63).

Antibodies. For detection of proteins of interest on immunoblots we used an anti-PSTAIR antibody to detect Cdk (Fig. 10A; Abcam, Cat#: ab10345) and an anti-hCBS polyclonal antibody to detect human and yeast CBS proteins (Fig. 10A; SantaCruz, Cat#:46830). Secondary antibodies were from Pierce. All antibodies were used at the dilutions recommended by the manufacturers.

3.2 Methods for drug treatment analysis

Yeast strains. For our primary analysis, we used the *S. cerevisiae* strain JTY2953 (*MATa pdr5::TRP1 snq2::hisG ade2-101 his3-Δ200 leu2-Δ1 lys2-801am trp1-Δ63 ura3–5*2; a generous gift from Dr. Paul deFigueiredo, Texas A&M University). For the elutriation experiments in Fig. 4 we used the diploid strain BY4743 (*MATa/α his3Δ1/his3Δ1 leu2Δ0 /leu2Δ0 lys2Δ0/LYS2 MET15/met15Δ0 ura3Δ0/ura3Δ0*; commercially available from Open Biosystems). For all other experiments, we used the haploid strain BY4741 (MATa *his3Δ1 leu2Δ0 met15Δ0 ura3Δ0*; commercially available from Open Biosystems).

Media and culture conditions. In all experiments, strains were cultured at 30 °C in YPD (1% yeast extract, 2% peptone, 2% dextrose). For our primary analysis with the JTY2953 strain, overnight cultures were diluted 1:200 and aliquoted into 96-well plates, 198 μl per well. To each well we then added 2 μl of a drug stock solution (2 mg/ml in DMSO), resulting in a final drug concentration of 20 μg/ml. At the four corner wells of each 96-well plate, the cultures were treated with DMSO only. These cultures served as the mock-treated reference samples. The plates were then placed at 30 °C and incubated standing for 6-7 h. Each of the 200 μl cultures were then transferred to microcentrifuge tubes containing 500 μl ethanol, and sonicated for 5 s. For the experiments where the drugs were added in dividing JTY2953 cells, the overnight cultures were diluted 1:400 and incubated for 3 h at 30 °C. We then added the drugs of interest and incubated the plates at 30 °C for another 6 h before fixing the samples in ethanol. For DNA content measurements in BY4741 cells, which proliferate faster than JTY2953 cells do, overnight cultures were diluted 1:400, cultured for 2.16 h before we added the drugs of interest, and then cultured for another 4.33 h before they were fixed in ethanol.

Cell size determinations. To obtain size distributions from asynchronous cultures, overnight cultures of BY4743 cells were diluted 1:500 in fresh medium, and incubated for 2 h at 30 °C. We then added the drugs of interest and incubated at 30 °C for another 4 h. Cell size was then measured with a Beckman Z2 Channelyzer. For each sample we analyzed, we obtained size distributions from two different dilutions of cells. The

average of the geometric mean of each size distribution was recorded. We used the Accucomp Beckman software package to obtain the statistics of each size distribution.

Measurements of critical size and growth rate from elutriated cultures. For isolation of early G1 daughter cells, cultures were grown in YPD at 30°C to a density of ~1-5x10^7 cells/ml, then fractionated with a Beckman JE-5.0 elutriator as described previously (7). Early fractions containing predominantly (>95%) small unbudded cells were collected by centrifugation, re-suspended in fresh medium and aliquoted in three separate flasks. To each flask, we then added as indicated rapamycin (at 0.1 μg/ml), gemfibrozil (at 50 μg/ml), or DMSO alone. After testing several doses of each drug and measuring the DNA content, we decided to use these concentrations because they were the lowest ones that resulted in consistently pronounced effects in this strain background. The cultures were incubated at 30 °C. Every 20 min we monitored the percentage of budded cells and cell size. The "critical size" is the size at which 50% of the cells have budded in these experiments, and it was calculated as we described elsewhere (7). To calculate "growth rate" assuming exponential growth, we plotted the natural log (ln) of cell size as a function of time (in h), see Fig. A-10. We fit the data to a straight line using the regression function in Microsoft Excel. From the slope of the line, we obtained the specific rate of cell size increase constant (k, in h^{-1}). The average of all experiments (n=3) for each treatment was then calculated, along with the associated standard deviation.

Staining for DNA content analyses. Cells were fixed and stained as in the genetic deletion analysis protocol (section 3.1), except they were stained overnight in 0.5 ml staining solution containing 50 mM sodium citrate pH 7.0, 0.25 mg/ml RNaseA, and 1 μM SYTOX Green (Molecular Probes).

Flow cytometry data acquisition, deposition and analysis. Data were acquired, deposited, and analyzed as in the genetic deletion analysis protocol (section 3.1), with exceptions as follow. Gates were centered near FSC ~100 and FL2-A ~300 and contained all events of sufficient contiguity as defined by the default autogating parameters, on average ~95% of total. Model fits that did not accurately represent experimental data were assessed primarily by root mean square (RMS) error and ratio of mean fluorescence intensities (MFI, calculated from the FL2-A parameter) of the G2/M vs. G1 peaks. Automated unconstrained analyses that yielded extremes in these parameters, or extremes in %G1 or S-phase components of the model fit, were manually constrained by application of the median G2/G1 MFI ratio and a G1 MFI position that minimized the resulting overall RMS. All model fits were visually inspected in order to confirm the accuracy of the fit. Unquantifiable data was excluded from further analysis. Experimental data and correlations are provided in the searchable spreadsheet available as Dataset C-2. Raw data files can be freely accessed at Cytobank (www.cytobank.org) and are found in the public experiments "Yeast DNA Content Project - DRUG - INCLUDED" and "Yeast DNA Content Project - DRUG -EXCLUDED".

Proliferation assays. Yeast strain BY4741 was grown overnight at 30 °C in a 1 ml YPD starter culture, then diluted 1:200 into fresh YPD in the presence or absence of drug. 200 µl volumes were aliquoted into clear flat-bottom 96-well sterile cell culture plates (Thermo Scientific, Nunc MicroWell Plate 167008), and the absorbance at 600 nm was measured hourly using a Tecan infinite 200Pro plate reader, after one minute of 3.5 mm orbital shaking to re-suspend cells. Plates were incubated standing at 30 °C in between measurements. Absorbances were blanked post-measurement against wells containing media and DMSO alone. For combination assays, cells were treated with drug at the time of initial reseeding, at a final DMSO concentration of 1.24% throughout, aliquoted immediately into 96-well plates for reading of absorbance, and followed as described above. Growth constants were calculated using a best fit for exponential growth incorporating time points from 2 h through 6 h. For order of addition experiments, cells were reseeded at 1:200 into fresh YPD in a culture tube, cultured standing at 30 °C with hourly re-suspension for 3 h, then divided into three tubes and treated with the first drug (200 µM) or DMSO-only control, at a final DMSO concentration of 0.62% throughout. Following an additional 3 h of incubation at 30 °C, the primary treated cultures were washed twice with fresh YPD at 30 °C, re-suspended in the same, and further divided for treatment with the second drug, as above, resulting in nine total temporal combinations of vehicle, gemfibrozil, and fluoxetine. Growth constants were calculated as above from 0 h through 6 h.

Drugs. The FDA-approved library was purchased from Enzo (Cat. #: BML-2841). Artemisinin was from Enzo (Cat. #: ALX-350-219), gemfibrozil from Sigma (Cat. #: G9518), while chlorpromazine (Cat. #: 101077-482), fluoxetine (Cat. #: 89160-860) and clinafloxacin (Cat. #: 89150-368) were purchased through VWR International. All drug stock solutions were in DMSO.

4. SUMMARY AND CONCLUSIONS

Our results provide a comprehensive picture of the genetic requirements for the proper timing of initiation of cell division. The data we present raise several questions, and we discuss their implications and significance in the context of prevailing models of cell-cycle control mechanisms.

4.1 Discussion of genetic deletion analysis

Why do most gene deletions that affect cell-cycle progression lead to a G1 delay? We think that this likely reflects the fact that cells commit to initiation of cell division in the G1 phase. It is reasonable to expect that extensive regulatory networks contribute to such a critical cellular transition, perhaps more so than for other cell-cycle transitions. Interestingly, inactivation of the majority of essential genes also leads to a G1 arrest (118). Furthermore, the strong requirement of protein synthesis for START completion (2, 42, 69, 81, 83, 94, 95, 107), and the large number of essential and non-essential genes involved in protein synthesis, also partially explains why most gene deletions that affect the cell cycle lead to a G1 delay.

Is there a critical size threshold for initiation of cell division in yeast? This question has been highly debated (see (65, 113) for related commentaries), especially when yeast is contrasted with animal model systems. Our study does *not* address this question. The

debate about whether there is a critical threshold for initiation of cell division centers on whether cell size increases in a linear, or in an exponential fashion (19, 65, 106, 113). In several experiments, we monitored cell size increases as a function of time in synchronous cultures. However, our data points are of insufficient resolution to distinguish between an exponential vs. linear mode of growth (see Fig. A-7 and Materials and Methods). Note that this limitation does not in any way affect our conclusions about the relative rates of growth of different strains. In fact, when we compare strains with similar overall size distributions (see Fig. A-2A) the relative "growth rates" we obtain are the same, whether cells increase in size exponentially or not. Even in the case of strains with very different size distributions (e.g., wild type vs. *sfp1Δ* cells, see Fig. A-2B and Fig. 5), the results are qualitatively similar, regardless of the pattern of growth. Nonetheless, in our study we have monitored and incorporated in our calculations the "critical size" at which cells initiate their division. From these experiments and similar others we published previously (see Fig. A-3, A-7, A-8, A-9 and (6, 7, 43)), the "critical size" is a highly reproducible parameter. Hence, in accordance with numerous other reports, it is our opinion that any strain growing in a given medium has to reach a critical size characteristic of that strain and medium.

Why do most gene deletions that affect cell-cycle progression not affect cell size?

Our genome-wide data unequivocally show little correlation between %G1 and cell size (see Fig. 4, A-4, A-5). Thus, although reaching a critical size threshold for initiation of cell division contributes to the timing of START, the most reasonable conclusion from

our data is that genetic determinants of size control mechanisms are neither the sole nor the major factor determining the timing of initiation of cell division in dividing cells. This is a key finding of our study, which stands in marked contrast to previous approaches that used cell size alterations as a means to identify START regulators (52). In our opinion, monitoring the length of the G1 phase reflects the timing of START far more accurately than monitoring cell size. We expand more on this issue next, when we discuss the role of ribosome biogenesis and the behavior of wild type cells in different nutrients.

Does ribosome biogenesis promote or delay START in yeast? The behavior of strains lacking genes involved in ribosome biogenesis and protein synthesis exemplifies the different interpretations about the timing of START, depending on whether the focus is on the length of G1 (this study), or on cell size (52, 53). We will discuss the phenotypes of *sfp1Δ* cells, because we examined them (see Fig. 5) with the same methods and under the same conditions as in previous studies by Jorgensen et al (53). The parameters we obtained are in complete agreement with those of Jorgensen et al (53): *sfp1Δ* cells divide at a greatly reduced cell size, grow much more slowly than wild type cells, and they are also born small. Jorgensen et al focused on their small critical size and concluded that START was accelerated in *sfp1Δ* cells and other strains lacking genes involved in ribosome biogenesis (53). Instead, we took into account not only their small critical size, but also their extremely slow growth rate and small birth size (see Fig. 5, A-2, A-7). We conclude that START must be severely delayed in *sfp1Δ* cells, because these cells have

such an expanded G1. If one focuses only on the small critical size of *sfp1Δ* cells, it may seem that START is accelerated. However, we think it is more accurate to describe these cells simply as small and severely growth-impaired. Loss of Sfp1p delays START to such an extent that during the time *sfp1Δ* cells spend in G1, their wild type counterparts would have initiated several new rounds of cell division.

Not all gene deletions that affect ribosome biogenesis prolong G1 and those that do may differ quantitatively and qualitatively in their impact (Fig. 5, 6). Overall, however, the G1 phase is prolonged in many ribosome biogenesis mutants (see Dataset C-1). Because of their lengthened G1, we conclude that START is delayed in strains lacking non-essential ribosomal components or factors that regulate protein synthesis. This interpretation is consistent with the terminal G1 arrest of essential genes involved in the same processes (118), and with the strong delay of START upon inactivation of rRNA processing in yeast (2). For these reasons, we conclude that gene deletions that impair ribosome biogenesis delay START, and that in dividing wild type yeast cells, ribosome biogenesis *promotes* START. This conclusion also agrees with extensive evidence from animal cells that increased ribosomal biogenesis (by Myc and other oncogenes) promotes initiation of cell division (17, 36, 72, 109).

Does the length of the G1 phase accurately reflect the timing of START? Obviously, completion of START and commitment to a new round of cell division precedes the actual end of the G1 phase, when cells initiate DNA replication (30, 83). Mutants in processes that molecularly link START with DNA replication (e.g., *cdc34* cells (110)),

may complete START, but they are unable to initiate DNA replication. These rare exceptions notwithstanding, we see no compelling reason that invalidates using the length of the G1 phase as an accurate metric of the timing of START. This is supported further by the behavior of dividing wild type cells in different growth conditions. Poor growth conditions greatly prolong G1, whereas the time required to transit the remaining cell-cycle phases is unaffected (50). In steady-state chemostat cultures, where growth rate can be altered independently of nutrient composition, the lower the growth rate is, the longer the cells stay in G1, delaying START completion (12, 43), while cell size remains largely unaffected (12, 37). Nutrients also affect the critical size threshold. Cells dividing in poor carbon sources typically are small, but they also have a slow growth rate and a long G1 (105), resembling ribosome biogenesis mutants with a delayed START.

We would like to clarify that, in all of the above examples we discussed, we considered continuously dividing populations, without media changes. In a nutritional up-shift, from poor to rich media, G1 is transiently prolonged, probably until cells reach the new larger "critical size" characteristic of the rich medium (49). During this short temporal window, in the first cell cycle as cells transit from the poor medium to the new richer one, genetic control of the "critical size" threshold likely prolongs G1 and delays START by increasing the critical size threshold (53, 54). In subsequent cell cycles however, despite the larger "critical size" cells have to attain in that richer medium, the cells are born larger and grow faster, resulting in a short G1 and accelerated START.

What could be the benefit of the small critical size observed in poor nutrients? It has been argued that the plasticity of critical size thresholds may allow yeast cells to "best compete for limited and fluctuating resources" (54). This is reasonable, if one keeps in mind the two competing objectives of all proliferating cells: i) Ensure that growth requirements are met before initiating a new round of cell division; ii) At the same time, exploit all the available nutrients to divide as quickly and as many times as possible. Perhaps, with their smaller birth size and slower growth rate, which lengthen G1, cells in poor nutrients satisfy the first objective. Then, as they progress in G1, cells have to reach a smaller critical size, alleviating a little bit the overall delay in initiating a new round of cell division in poor nutrients.

Implications for our understanding of genetic networks that control initiation of cell division. Overall, our results increase the number of gene deletions that delay G1, as listed currently in the *Saccharomyces Genome Database*, by more than 3-fold. Even if one excludes genes involved in ribosome biogenesis, we still uncovered >100 genes required for the timely initiation of cell division (see Dataset C-1). Most of the genes we identified do not affect cell size. As a result, these genes were not identified in previous attempts to find regulators of START. Hence, our findings greatly expand and reshape our view of START. We followed up one such gene we identified in this study, Cys4p (CBS). CBS is a key metabolic enzyme, associated with disease in humans, with conserved functions between yeast and humans. Indeed, human CBS complements yeast lacking Cys4p (62). Hence, the role of CBS in cell division we described in yeast may be

significant for human biology. The systematic identification of non-essential regulators of START we described here will be the basis for further insight into the control of cell division in yeast and other organisms. It enables future studies to define how many pathways affect START, which factors operate within each pathway, and the extent of interactions between pathways.

4.2 Discussion of drug treatment analysis

What is the significance of the gemfibrozil-fluoxetine interaction? Because of the novel and opposing cell-cycle effects of the individual drugs, we subsequently examined the combined effects of gemfibrozil and fluoxetine on cell proliferation and found that gemfibrozil suppresses the proliferative defect resulting from fluoxetine treatment. Understanding the basis of the interaction between gemfibrozil and fluoxetine would require a mechanistic understanding of their function in yeast cells. We would like to note that the suppressive interaction between the two compounds could be unrelated to their cell-cycle effects. For example, gemfibrozil might induce expression of proteins that do not interfere with cell-cycle progression, but may cause fluoxetine resistance. Fluoxetine is an anti-depressant thought to act as a serotonin-specific reuptake inhibitor (116). Hence, the effects we described for fluoxetine in yeast appear to result from some other mechanism. Similarly, nuclear receptors of the PPARα/RXR type, the target of gemfibrozil, are thought to be unique to animals and sponges (29, 115), but ancestral analogs may exist in yeast (78). Nonetheless, although the effects of fluoxetine and

gemfibrozil on yeast cells we described above likely represent off-target modes of action, they may act similarly in other eukaryotic organisms, including humans. In conclusion, our results suggest that monitoring the effects of drugs on cell-cycle progression reveals unexpected cellular roles of widely prescribed compounds. Finally, although we did not test all possible combinations of the compounds that affected cell-cycle progression, at least in the case of gemfibrozil and fluoxetine, our results suggest that combining such compounds may also be an effective strategy to identify novel drug interactions.

4.3 Future investigations

The networks of physical and functional interactions we have described (Fig. 7 and 8) are limited by *existing* descriptions of these interactions from the curated body of literature. Since our results implicate many additional, previously unidentified genes in regulation of cell-cycle progression, including genes of unknown function, it is important that a network of epistatic genetic interactions specific to the phenotypes we describe be established as a framework for ultimate elucidation of the pathways controlling this process. This will be accomplished through production of homozygous diploid double mutant strains representing key deletions from our current dataset, which will be selected based on phenotype strength, perceived significance of currently described roles and/or interactions, and existing annotations or sequence data which suggest potentially important molecular role(s). These resulting strains will be analyzed with methods similar to those described here, and internally compared to the single

deletions in type and degree of effect. In the extent of this network refinement, we are limited only by the extent of our technical and temporal resources. Additional targeted experiments have been and will continue to be performed in order to more fully describe the effects of specific gene deletions, with a goal of ultimately describing the molecular and biochemical activities and interactions suggested by existing functional and new genetic networks.

Likewise, additional drugs and drug combinations of interest will be identified, both from our existing data and from future expansions of this set derived from experiments with larger panels. Even though we anticipate that many of the effects observed in yeast will also apply to higher eukaryotes, it is important to confirm this in additional model systems. To this end, experiments in animal models are already underway, and preliminary data indicate generally conserved effects, bolstering the likelihood that there are conserved mechanisms and demonstrating the applicability of these yeast data to issues of health and therapeutics.

In summary, in addition to challenging and refining previous models for factor identification, we have already significantly expanded the list of genes and drugs that affect cell-cycle progression. We therefore conclude that measurement of DNA content in yeast is a valid and powerful way to streamline identification of genetic regulators and pharmaceutical modulators of the eukaryotic cell cycle, and anticipate that this approach and the data we present here will both serve as foundations for future discoveries.

REFERENCES

1. Barbet NC, Schneider U, Helliwell SB, Stansfield I, Tuite MF, et al. 1996. TOR controls translation initiation and early G1 progression in yeast. Mol. Biol. Cell 7: 25-42.

2. Bernstein KA, Bleichert F, Bean JM, Cross FR, Baserga SJ. 2007. Ribosome Biogenesis Is Sensed at the Start Cell Cycle Checkpoint. Mol. Biol. Cell 18: 953-964.

3. Bhaumik SR & Green MR. 2002. Differential requirement of SAGA components for recruitment of TATA-box-binding protein to promoters in vivo. Mol. Cell. Biol. 22: 7365-7371.

4. Bjorklund M, Taipale M, Varjosalo M, Saharinen J, Lahdenpera J, et al. 2006. Identification of pathways regulating cell size and cell-cycle progression by RNAi. Nature 439: 1009-1013.

5. Blagosklonny MV, Pardee AB. 2002. The restriction point of the cell cycle. Cell Cycle 1: 103-110.

6. Blank HM, Gajjar S, Belyanin A, Polymenis M. 2009. Sulfur Metabolism Actively Promotes Initiation of Cell Division in Yeast. PLoS ONE 4: e8018.

7. Blank HM, Li C, Mueller JE, Bogomolnaya LM, Bryk M, et al. 2008. An increase in mitochondrial DNA promotes nuclear DNA replication in yeast. PLoS Genet. 4: e1000047.

8. Bloom J, Cross FR. 2007. Multiple levels of cyclin specificity in cell-cycle control. Nat. Rev. Mol. Cell Biol. 8: 149-160.

9. Boiteux S & Guillet M. 2004. Abasic sites in DNA: repair and biological consequences in Saccharomyces cerevisiae. DNA repair 3: 1-12.

10. Borisy AA, Elliott PJ, Hurst NW, Lee MS, Lehar J, et al. 2003. Systematic discovery of multicomponent therapeutics. Proc. Natl. Acad. Sci. U. S. A. 100: 7977-7982.

11. Bouquin N, Barral Y, Courbeyrette R, Blondel M, Snyder M & Mann C. 2000. Regulation of cytokinesis by the Elm1 protein kinase in Saccharomyces cerevisiae. J. Cell Sci. 113: 1435-1445.

12. Brauer MJ, Huttenhower C, Airoldi EM, Rosenstein R, Matese JC, et al. 2008. Coordination of growth rate, cell cycle, stress response, and metabolic activity in yeast. Mol. Biol. Cell 19: 352-367.

13. Caminero JA, Sotgiu G, Zumla A, Migliori GB. 2010. Best drug treatment for multidrug-resistant and extensively drug-resistant tuberculosis. Lancet Infectious Dis. 10: 621-629.

14. Campsteijn C, Wijnands-Collin A-MJ & Logie C. 2007. Reverse genetic analysis of the yeast RSC chromatin remodeler reveals a role for RSC3 and SNF5 homolog 1 in ploidy maintenance. PLoS Genet. 3: e92.

15. Carter BL, Jagadish MN. 1978. Control of cell division in the yeast Saccharomyces cerevisiae cultured at different growth rates. Exp. Cell Res. 112: 373-383.

16. Carter BL, Sudbery PE. 1980. Small-sized mutants of Saccharomyces cerevisiae. Genetics 96: 561-566.

17. Chan JC, Hannan KM, Riddell K, Ng PY, Peck A, et al. 2011. AKT Promotes rRNA Synthesis and Cooperates with c-MYC to Stimulate Ribosome Biogenesis in Cancer. Science Signaling 4: ra56.

18. Cherest H, Thomas D, Surdin-Kerjan Y. 1993. Cysteine biosynthesis in Saccharomyces cerevisiae occurs through the transsulfuration pathway which has been built up by enzyme recruitment. J. Bacteriol. 175: 5366-5374.

19. Conlon I, Raff M. 2003. Differences in the way a mammalian cell and yeast cells coordinate cell growth and cell-cycle progression. J. Biol. 2: 7.

20. Costanzo M, Nishikawa JL, Tang X, Millman JS, Schub O, et al. 2004. CDK activity antagonizes Whi5, an inhibitor of G1/S transcription in yeast. Cell 117: 899-913.

21. Cross FR. 1988. DAF1, a mutant gene affecting size control, pheromone arrest, and cell cycle kinetics of Saccharomyces cerevisiae. Mol. Cell. Biol. 8: 4675-4684.

22. De Bruin RAM, McDonald WH, Kalashnikova TI, Yates J, Wittenberg C. 2004. Cln3 activates G1-specific transcription via phosphorylation of the SBF bound repressor Whi5. Cell 117: 887-898.

23. Dennis RA & McCammon MT. 1999. Acn9 is a novel protein of gluconeogenesis that is located in the mitochondrial intermembrane space. Eur. J. Biochem./FEBS 261: 236-243.

24. Donachie WD. 1968. Relationship between cell size and time of initiation of DNA replication. Nature 219: 1077-1079.

25. Doncic A, Falleur-Fettig M, Skotheim JM. 2011. Distinct interactions select and maintain a specific cell fate. Mol. Cell 43: 528-539.

26. Edwards MC, Liegeois N, Horecka J, DePinho RA, Sprague GFJ, et al. 1997. Human CPR (Cell Cycle Progression Restoration) genes impart a Far- phenotype on yeast cells. Genetics 147: 1063-1076.

27. Enokido Y, Suzuki E, Iwasawa K, Namekata K, Okazawa H, et al. 2005. Cystathionine beta-synthase, a key enzyme for homocysteine metabolism, is preferentially expressed in the radial glia/astrocyte lineage of developing mouse CNS. FASEB J. 19: 1854-1856.

28. Epstein CB, Cross FR. 1994. Genes that can bypass the CLN requirement for Saccharomyces cerevisiae cell cycle START. Mol. Cell. Biol. 14: 2041-2047.

29. Escriva H, Delaunay F, Laudet V. 2000. Ligand binding and nuclear receptor evolution. BioEssays 22: 717-727.

30. Eser U, Falleur-Fettig M, Johnson A, Skotheim JM. 2011. Commitment to a Cellular Transition Precedes Genome-wide Transcriptional Change. Mol. Cell 43: 515-527.

31. Fingerman I, Nagaraj V, Norris D, Vershon AK. 2003. Sfp1 plays a key role in yeast ribosome biogenesis. Eukaryot. Cell 2: 1061-1068.

32. Formenti LR, Kielland-Brandt MC. 2011. Sensitivity to lovastatin of Saccharomyces cerevisiae strains deleted for pleiotropic drug resistance (PDR) genes. J. Mol. Microb. Biotech. 20: 191-195.

33. Fowler B. 2005. Homocysteine: overview of biochemistry, molecular biology, and role in disease processes. Semin. Vasc. Med. 5: 77-86.

34. Gavin AC, Aloy P, Grandi P, Krause R, Boesche M, et al. 2006. Proteome survey reveals modularity of the yeast cell machinery. Nature 440: 631-636.

35. Giaever G, Chu AM, Ni L, Connelly C, Riles L, et al. 2002. Functional profiling of the Saccharomyces cerevisiae genome. Nature 418: 387-391.

36. Grewal SS, Li L, Orian A, Eisenman RN, Edgar BA. 2005. Myc-dependent regulation of ribosomal RNA synthesis during Drosophila development. Nat. Cell Biol. 7: 295-302.

37. Guo J, Bryan BA, Polymenis M. 2004. Nutrient-specific effects in the coordination of cell growth with cell division in continuous cultures of Saccharomyces cerevisiae. Arch. Microbiol. 182: 326-330.

38. Haase SB, Lew DJ. 1997. Flow cytometric analysis of DNA content in budding yeast. Methods Enzymol. 283: 322-332.

39. Hadwiger JA, Wittenberg C, Mendenhall MD, Reed SI. 1989. The Saccharomyces cerevisiae CKS1 gene, a homolog of the Schizosaccharomyces pombe suc1+ gene, encodes a subunit of the Cdc28 protein kinase complex. Mol. Cell. Biol. 9: 2034-2041.

40. Hadwiger JA, Wittenberg C, Richardson HE, de Barros Lopes M, Reed SI. 1989. A family of cyclin homologs that control the G1 phase in yeast. Proc. Natl. Acad. Sci. U. S. A. 86: 6255-6259.

41. Hanna JS, Kroll ES, Lundblad V & Spencer FA. 2001. Saccharomyces cerevisiae CTF18 and CTF4 are required for sister chromatid cohesion. Mol. Cell. Biol. 21: 3144-3158.

42. Hartwell LH, Unger MW. 1977. Unequal division in Saccharomyces cerevisiae and its implications for the control of cell division. J. Cell Biol. 75: 422-435.

43. Henry KA, Blank HM, Hoose SA, Polymenis M. 2010. The unfolded protein response is not necessary for the G1/S transition, but it is required for chromosome maintenance in Saccharomyces cerevisiae. PLoS ONE 5: e12732.

44. Hoepfner D, Schaerer F, Brachat A, Wach A & Philippsen P. 2002. Reorientation of mispositioned spindles in short astral microtubule mutant spc72Delta is dependent on spindle pole body outer plaque and Kar3 motor protein. Mol. Biol. Cell 13: 1366-1380.

45. Hoose SA, Rawlings JA, Kelly MM, Leitch MC, Ababneh QO, et al. 2012. A systematic analysis of cell cycle regulators in yeast reveals that most factors act independently of cell size to control initiation of division. PLoS Genet. 8: e1002590.

46. Huggins DJ, Venkitaraman AR, Spring DR. 2011. Rational methods for the selection of diverse screening compounds. ACS Chem. Biol. 6: 208-217.

47. Hughes TR, Roberts CJ, Dai H, Jones AR, Meyer MR, et al. 2000. Widespread aneuploidy revealed by DNA microarray expression profiling. Nat. Genet. 25: 333-337.

48. Jagadish MN, Carter BL. 1977. Genetic control of cell division in yeast cultured at different growth rates. Nature 269: 145-147.

49. Johnston GC, Ehrhardt CW, Lorincz A, Carter BL. 1979. Regulation of cell size in the yeast Saccharomyces cerevisiae. J. Bacteriol. 137: 1-5.

50. Johnston GC, Pringle JR, Hartwell LH. 1977. Coordination of growth with cell division in the yeast Saccharomyces cerevisiae. Exp. Cell Res. 105: 79-98.

51. Jordan PW, Klein F & Leach DRF. 2007. Novel roles for selected genes in meiotic DNA processing. PLoS Genet. 3: e222.

52. Jorgensen P, Nishikawa JL, Breitkreutz BJ, Tyers M. 2002. Systematic identification of pathways that couple cell growth and division in yeast. Science 297: 395-400.

53. Jorgensen P, Rupes I, Sharom JR, Schneper L, Broach JR, et al. 2004. A dynamic transcriptional network communicates growth potential to ribosome synthesis and critical cell size. Genes Dev. 18: 2491-2505.

54. Jorgensen P, Tyers M. 2004. How cells coordinate growth and division. Curr. Biol. 14: R1014-R1027.

55. Kaiser C, Michaelis S, Mitchell A. 1994. Methods in Yeast Genetics. Cold Spring Harbor: Cold Spring Harbor Laboratory Press.

56. Keller HU, Fedier A, Rohner R. 1995. Relationship between light scattering in flow cytometry and changes in shape, volume, and actin polymerization in human polymorphonuclear leukocytes. J. Leukocyte Biol. 58: 519-525.

57. Keyomarsi K, Sandoval L, Band V, Pardee AB. 1991. Synchronization of tumor and normal cells from G1 to multiple cell cycles by lovastatin. Cancer Res. 51: 3602-3609.

58. Killander D, Zetterberg A. 1965. A quantitative cytochemical investigation of the relationship between cell mass and initiation of DNA synthesis in mouse fibroblasts in vitro. Exp. Cell Res. 40: 12-20.

59. Kittler R, Pelletier L, Heninger AK, Slabicki M, Theis M, et al. 2007. Genome-scale RNAi profiling of cell division in human tissue culture cells. Nat. Cell Biol. 9: 1401-1412.

60. Koepp DM, Kile AC, Swaminathan S & Rodriguez-Rivera V. 2006. The F-box protein Dia2 regulates DNA replication. Mol. Biol. Cell 17: 1540-1548.

61. Kotecha N, Krutzik PO, Irish JM. 2010. Web-based analysis and publication of flow cytometry experiments. Current protocols in cytometry Chapter 10: Unit 10.17.

62. Kruger WD, Cox DR. 1994. A yeast system for expression of human cystathionine beta-synthase: structural and functional conservation of the human and yeast genes. Proc. Natl. Acad. Sci. U. S. A. 91: 6614-6618.

63. Kushnirov VV. 2000. Rapid and reliable protein extraction from yeast. Yeast 16: 857-860.

64. Kwan EX, Foss E, Kruglyak L & Bedalov A. 2011. Natural polymorphism in BUL2 links cellular amino acid availability with chronological aging and telomere maintenance in yeast. PLoS Genet. 7: e1002250.

65. Leslie M. 2011. How Does a Cell Know Its Size. Science 334: 1047-1048.

66. Makovets S, Herskowitz I & Blackburn EH. 2004. Anatomy and dynamics of DNA replication fork movement in yeast telomeric regions. Mol. Cell. Biol. 24: 4019-4031.

67. Marion RM, Regev A, Segal E, Barash Y, Koller D, et al. 2004. Sfp1 is a stress- and nutrient-sensitive regulator of ribosomal protein gene expression. Proc. Natl. Acad. Sci. U. S. A. 101: 14315-14322.

68. Mendenhall MD, al-Jumaily W, Nugroho TT. 1995. The Cdc28 inhibitor p40SIC1. Prog. Cell Cycle Res. 1: 173-185.

69. Moore SA. 1988. Kinetic evidence for a critical rate of protein synthesis in the Saccharomyces cerevisiae yeast cell cycle. J. Biol. Chem. 263: 9674-9681.

70. Niu W, Li Z, Zhan W, Iyer VR, Marcotte EM. 2008. Mechanisms of cell cycle control revealed by a systematic and quantitative overexpression screen in S. cerevisiae. PLoS Genet. 4: e1000120.

71. Ohya T, Maki S, Kawasaki Y & Sugino A. 2000. Structure and function of the fourth subunit (Dpb4p) of DNA polymerase epsilon in Saccharomyces cerevisiae. Nucl. Acids Res. 28: 3846-3852.

72. Oskarsson T, Trumpp A. 2005. The Myc trilogy: lord of RNA polymerases. Nat. Cell Biol. 7: 215-217.

73. Ozier-Kalogeropoulos O, Fasiolo F, Adeline MT, Collin J & Lacroute F. 1991. Cloning, sequencing and characterization of the Saccharomyces cerevisiae URA7 gene encoding CTP synthetase. Mol. Gen. Genet. 231: 7-16.

74. Padmanabha R, Gehrung S, Snyder M. 1991. The KNS1 gene of Saccharomyces cerevisiae encodes a nonessential protein kinase homologue that is distantly related to members of the CDC28/cdc2 gene family. Mol. Gen. Genet. 229: 1-9.

75. Pardee AB. 1974. A restriction point for control of normal animal cell proliferation. Proc. Natl. Acad. Sci. U. S. A. 71: 1286-1290.

76. Pardee AB. 1989. G1 events and regulation of cell proliferation. Science 246: 603-608.

77. Parks LW, Casey WM. 1995. Physiological implications of sterol biosynthesis in yeast. Annu. Review Microbiol. 49: 95-116.

78. Phelps C, Gburcik V, Suslova E, Dudek P, Forafonov F, et al. 2006. Fungi and animals may share a common ancestor to nuclear receptors. Proc. Natl. Acad. Sci. U. S. A. 103: 7077-7081.

79. Pirrone V, Thakkar N, Jacobson JM, Wigdahl B, Krebs FC. 2011. Combinatorial approaches to the prevention and treatment of HIV-1 infection. Antimicrob. Agents Ch 55: 1831-1842.

80. Polymenis M, Schmidt EV. 1997. Coupling of cell division to cell growth by translational control of the G1 cyclin CLN3 in yeast. Genes Dev. 11: 2522-2531.

81. Popolo L, Vanoni M, Alberghina L. 1982. Control of the yeast cell cycle by protein synthesis. Exp. Cell Res. 142: 69-78.

82. Prendergast JA, Murray LE, Rowley A, Carruthers DR, Singer RA, et al. 1990. Size selection identifies new genes that regulate Saccharomyces cerevisiae cell proliferation. Genetics 124: 81-90.

83. Pringle JR, Hartwell LH. 1981. The Saccharomyces cerevisiae cell cycle. In: Strathern JD, Jones EW, Broach JR, editors. The molecular biology of the yeast Saccharomyces. Cold Spring Harbor, NY: Cold Spring Harbor Laboratory Press. pp. 97-142.

84. Quazi F, Aitken SM. 2009. Characterization of the S289A,D mutants of yeast cystathionine beta-synthase. Biochim. Biophys. Acta 1794: 892-897.

85. Reed SI, Hadwiger JA, Richardson HE, Wittenberg C. 1989. Analysis of the Cdc28 protein kinase complex by dosage suppression. J. Cell Sci. Suppl. 12: 29-37.

86. Reid RJ, Gonzalez-Barrera S, Sunjevaric I, Alvaro D, Ciccone S, et al. 2011. Selective ploidy ablation, a high-throughput plasmid transfer protocol, identifies new genes affecting topoisomerase I-induced DNA damage. Genome Res. 21: 477-486.

87. Roth AF, Feng Y, Chen L & Davis NG. 2002. The yeast DHHC cysteine-rich domain protein Akr1p is a palmitoyl transferase. J. Cell Biol. 159: 23-28.

88. Roy A, Pahan K. 2009. Gemfibrozil, stretching arms beyond lipid lowering. Immunopharm. Immunot. 31: 339-351.

89. Sbia M, Parnell EJ, Yu Y, Olsen AE, Kretschmann KL, Voth WP & Stillman DJ. 2008. Regulation of the yeast Ace2 transcription factor during the cell cycle. J. Biol. Chem. 283: 11135-11145.

90. Schaechter M, Maaloe O, Kjeldgaard NO. 1958. Dependency on medium and temperature of cell size and chemical composition during balanced grown of Salmonella typhimurium. J. Gen. Microbiol. 19: 592-606.

91. Schaerer F, Morgan G, Winey M & Philippsen P. 2001. Cnm67p is a spacer protein of the Saccharomyces cerevisiae spindle pole body outer plaque. Mol. Biol. Cell 12: 2519-2533.

92. Shan X, Kruger WD. 1998. Correction of disease-causing CBS mutations in yeast. Nat. Genet. 19: 91-93.

93. Sharma SV, Haber DA, Settleman J. 2010. Cell line-based platforms to evaluate the therapeutic efficacy of candidate anticancer agents. Nat. Rev. Cancer 10: 241-253.

94. Shilo B, Riddle VG, Pardee AB. 1979. Protein turnover and cell-cycle initiation in yeast. Exp. Cell Res. 123: 221-227.

95. Shilo B, Simchen G, Pardee AB. 1978. Regulation of cell-cycle initiation in yeast by nutrients and protein synthesis. J. Cell Physiol. 97: 177-187.

96. Skotheim JM, Di Talia S, Siggia ED, Cross FR. 2008. Positive feedback of G1 cyclins ensures coherent cell cycle entry. Nature 454: 291-296.

97. Slater ML. 1977. Cell Cycle of Saccharomyces cerevisiae in Populations Growing at Different Rates. Proc. Natl. Acad. Sci. U. S. A. 74: 3850-3854.

98. Smoot ME, Ono K, Ruscheinski J, Wang PL, Ideker T. 2011. Cytoscape 2.8: new features for data integration and network visualization. Bioinformatics 27: 431-432.

99. Sopko R et al. 2006. Mapping pathways and phenotypes by systematic gene overexpression. Mol. Cell 21: 319-330.

100. Stark C, Breitkreutz BJ, Chatr-Aryamontri A, Boucher L, Oughtred R, et al. 2011. The BioGRID Interaction Database: 2011 update. Nucleic Acids Res. 39: D698-D704.

101. Stevenson LF, Kennedy BK, Harlow E. 2001. A large-scale overexpression screen in Saccharomyces cerevisiae identifies previously uncharacterized cell cycle genes. Proc. Natl. Acad. Sci. U. S. A. 98: 3946-3951.

102. Sudbery PE, Goodey AR, Carter BL. 1980. Genes which control cell proliferation in the yeast Saccharomyces cerevisiae. Nature 288: 401-404.

103. Surana U, Robitsch H, Price C, Schuster T, Fitch I, et al. 1991. The role of CDC28 and cyclins during mitosis in the budding yeast S. cerevisiae. Cell 65: 145-161.

104. Tong AH, Lesage G, Bader GD, Ding H, Xu H, et al. 2004. Global mapping of the yeast genetic interaction network. Science 303: 808-813.

105. Tyson CB, Lord PG, Wheals AE. 1979. Dependency of Size of Saccharomyces cerevisiae Cells on Growth rate. J. Bacteriol. 138: 92-98.

106. Tzur A, Kafri R, LeBleu VS, Lahav G, Kirschner MW. 2009. Cell growth and size homeostasis in proliferating animal cells. Science 325: 167-171.

107. Unger MW, Hartwell LH. 1976. Control of cell division in Saccharomyces cerevisiae by methionyl-tRNA. Proc. Natl. Acad. Sci. U. S. A. 73: 1664-1668.

108. Vaisica JA, Baryshnikova A, Costanzo M, Boone C & Brown GW. 2011. Mms1 and Mms22 stabilize the replisome during replication stress. Mol. Biol. Cell 22: 2396-2408.

109. Van Riggelen J, Yetil A, Felsher DW. 2010. MYC as a regulator of ribosome biogenesis and protein synthesis. Nat. Rev. Cancer 10: 301-309.

110. Verma R, Feldman RM, Deshaies RJ. 1997. SIC1 is ubiquitinated in vitro by a pathway that requires CDC4, CDC34, and cyclin/CDK activities. Mol. Biol. Cell 8: 1427-1437.

111. Wang L, Chen X, Tang B, Hua X, Klein-Szanto A, et al. 2005. Expression of mutant human cystathionine beta-synthase rescues neonatal lethality but not homocystinuria in a mouse model. Hum. Mol. Genet. 14: 2201-2208.

112. Watanabe M, Osada J, Aratani Y, Kluckman K, Reddick R, et al. 1995. Mice deficient in cystathionine beta-synthase: animal models for mild and severe homocyst(e)inemia. Proc. Natl. Acad. Sci. U. S. A. 92: 1585-1589.

113. Wells W. 2002. Does size matter? J. Cell Biol. 158: 1156-1159.

114. White MA, Riles L & Cohen BA. 2009. A systematic screen for transcriptional regulators of the yeast cell cycle. Genetics 181: 435-446.

115. Wiens M, Batel R, Korzhev M, Müller WEG. 2003. Retinoid X receptor and retinoic acid response in the marine sponge Suberites domuncula. J. Exp. Biol. 206: 3261-3271.

116. Wong DT, Horng JS, Bymaster FP, Hauser KL, Molloy BB. 1974. A selective inhibitor of serotonin uptake: Lilly 110140, 3-(p-Triflouromethylphenoxy)-N-Methyl-3-Phenylpropylamine. Life Sciences 15: 471-479.

117. Yompakdee C, Ogawa N, Harashima S & Oshima Y. 1996. A putative membrane protein, Pho88p, involved in inorganic phosphate transport in Saccharomyces cerevisiae. Mol. Gen. Genet. 251: 580-590.

118. Yu L, Pena Castillo L, Mnaimneh S, Hughes TR, Brown GW. 2006. A survey of essential gene function in the yeast cell division cycle. Mol. Biol. Cell 17: 4736-4747.

119. Zettel MF, Garza LR, Cass AM, Myhre RA, Haizlip LA, et al. 2003. The budding index of Saccharomyces cerevisiae deletion strains identifies genes important for cell cycle progression. FEMS Microbiol. Lett. 223: 253-258.

120. Zhang J, Schneider C, Ottmers L, Rodriguez R, Day A, et al. 2002. Genomic Scale Mutant Hunt Identifies Cell Size Homeostasis Genes in S. cerevisiae. Curr. Biol. 12: 1992-2001.

121. Zhang M-L et al. 2010. Yeast telomerase subunit Est1p has guanine quadruplex-promoting activity that is required for telomere elongation. Nat. Struct. Mol. Biol. 17: 202-209.

APPENDIX A

FIGURES

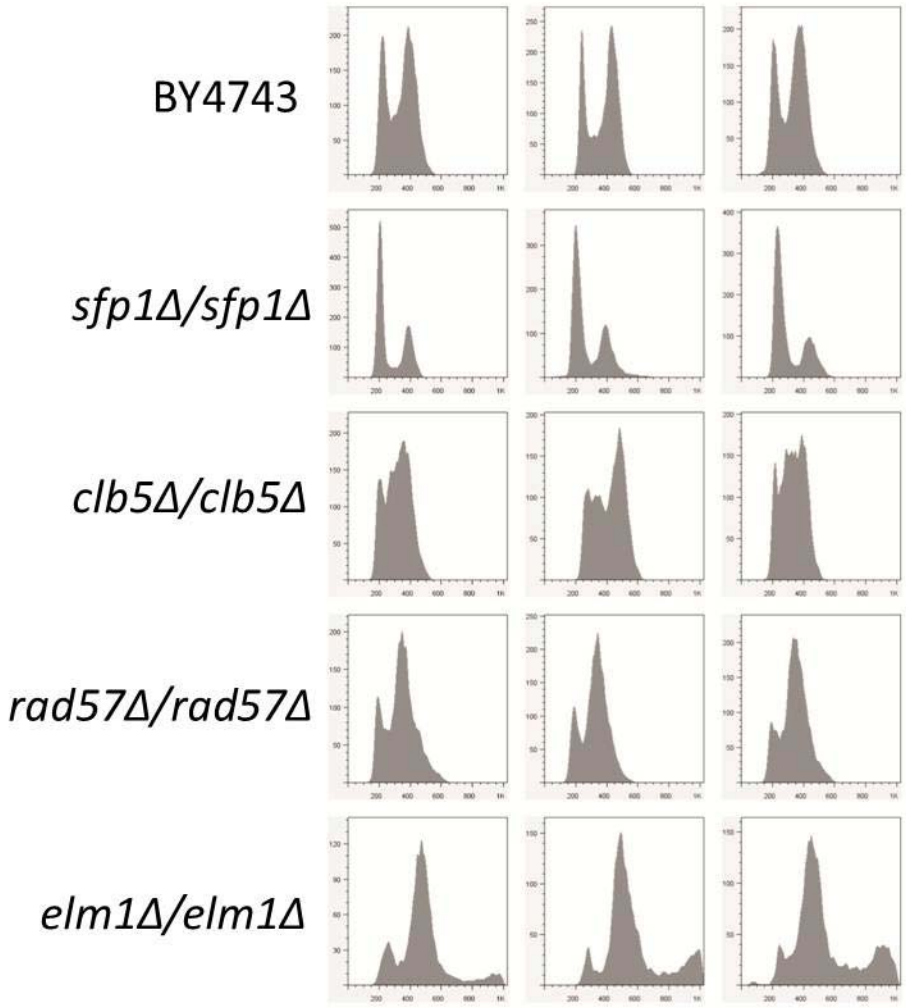

FIG A-1 Representative DNA content histograms. Three independent experiments of the indicated strains are shown in each case. Fluorescence is plotted on the x-axis, while the number of cells analyzed is on the y-axis. BY4743 is the wild type, diploid reference strain. *sfp1Δ/sfp1Δ*, or *rad57Δ/rad57Δ*, strains were from the "high G1", or "Low G1" sets, respectively. *clb5Δ/clb5Δ*, or *elm1Δ/elm1Δ*, strains have known roles during DNA replication, or cytokinesis and cell separation, respectively, giving rise to complex DNA content histograms that were not quantified.

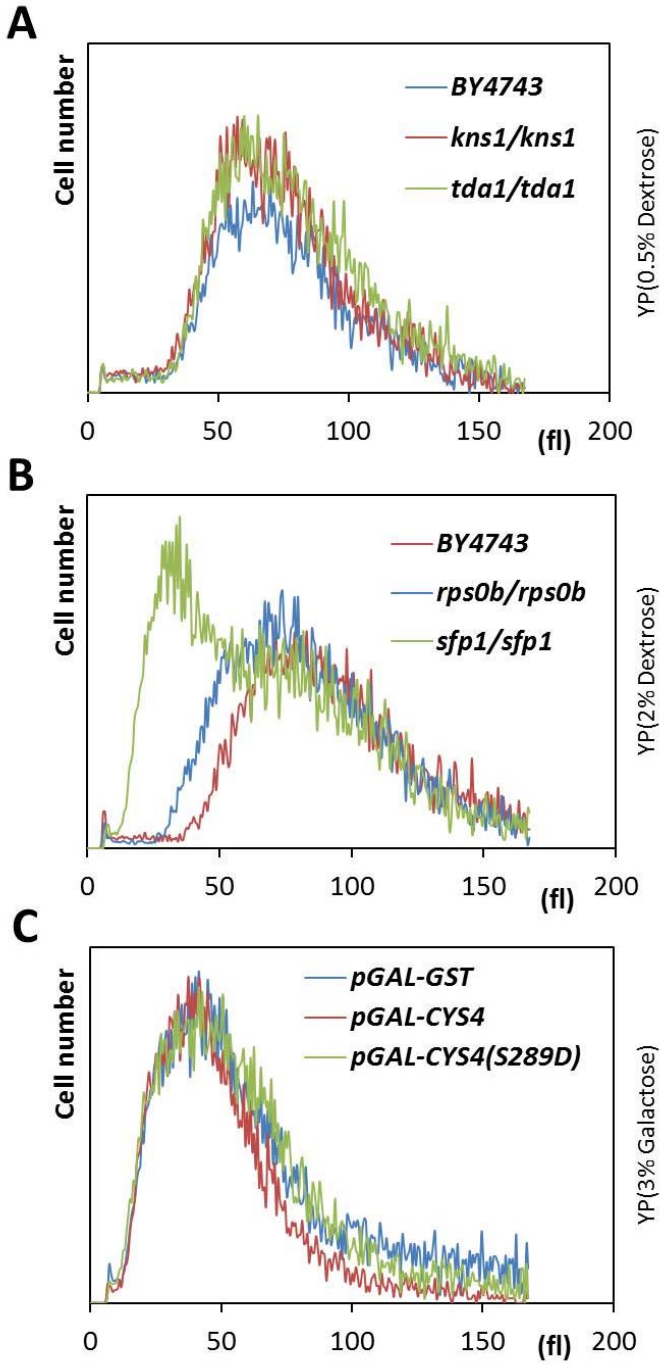

FIG A-2 Cell size distributions of asynchronous cultures. The cell size of the indicated cell populations was measured using a channelyzer (see Materials and Methods). Cell numbers are plotted on the y-axis and the x-axis indicates size (in fl). **A,** Size distributions of wild type (BY4743), *kns1Δ/kns1Δ* and *tda1Δ/tda1Δ* cells, cultured in YPD (0.5% Dextrose) medium. **B,** Size distributions of wild type (BY4743), *sfp1Δ/sfp1Δ* and *rps0bΔ/rps0bΔ* cells, cultured in YPD (2% Dextrose) medium. **C,** Size distributions of wild type *pGAL-GST*, *pGAL-CYS4*, *pGAL-CYS4(S289D)* cells, cultured in YPGal (3% Galactose) medium.

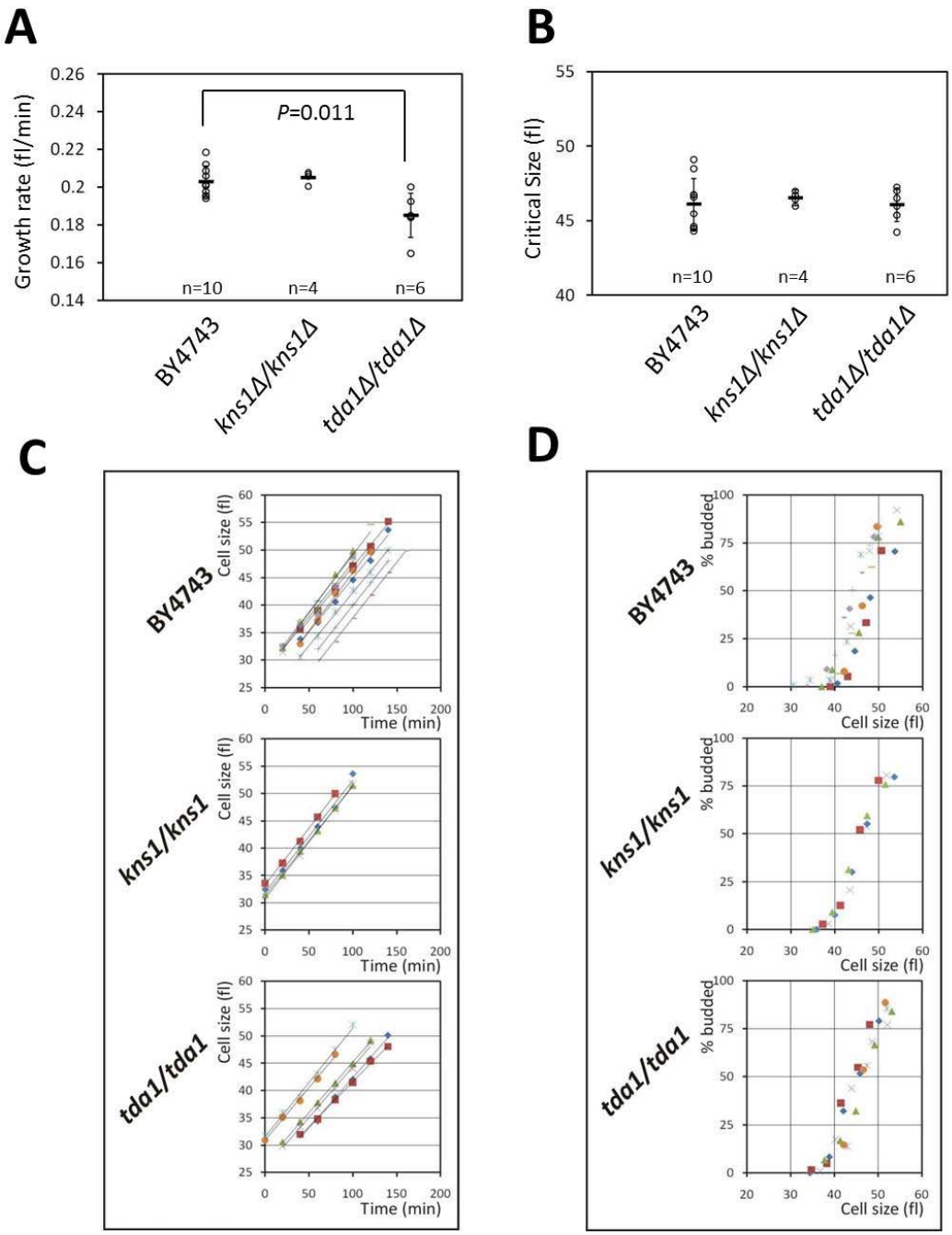

FIG A-3 Evaluating false negatives. (A) Rate of cell size increase (shown as growth rate, in fl/min) for the indicated strains was measured from synchronous cultures, in rich (YPD-0.5% Dextrose) medium, assuming linear growth. The average value for each strain is shown with a horizontal bar (± sd). (B) The critical cell size of the indicated strains (in fl), was measured from the same experiments shown in A. (C) Graphs from which we determined the growth rates shown in A. (D) Graphs from which we determined the percent of budded cells as a function of cell size, from the same elutriation experiments. The data points shown were from the linear portion of each experiment, when the percentage of budded cells began to increase, and used to determine the critical size for division we show in B.

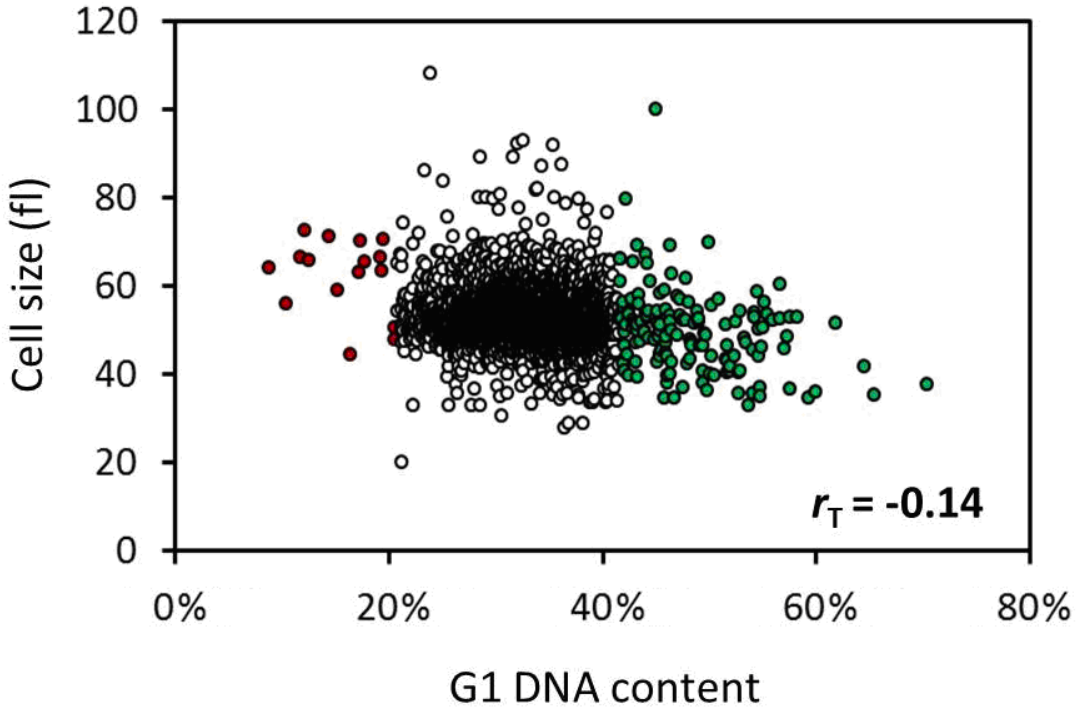

FIG A-4 Cell-cycle progression correlates weakly with cell size data from stationary phase growth. We plotted the %G1 (x-axis) from all the deletion strains we examined against the diploid median cell size (in fl, y-axis) data of Zhang et al (24), in stationary phase after growth on solid media. We calculated and displayed the *r* value as in Fig. 3. For every gene we included in this analysis, the values we used in this correlation are shown in Dataset C-1.

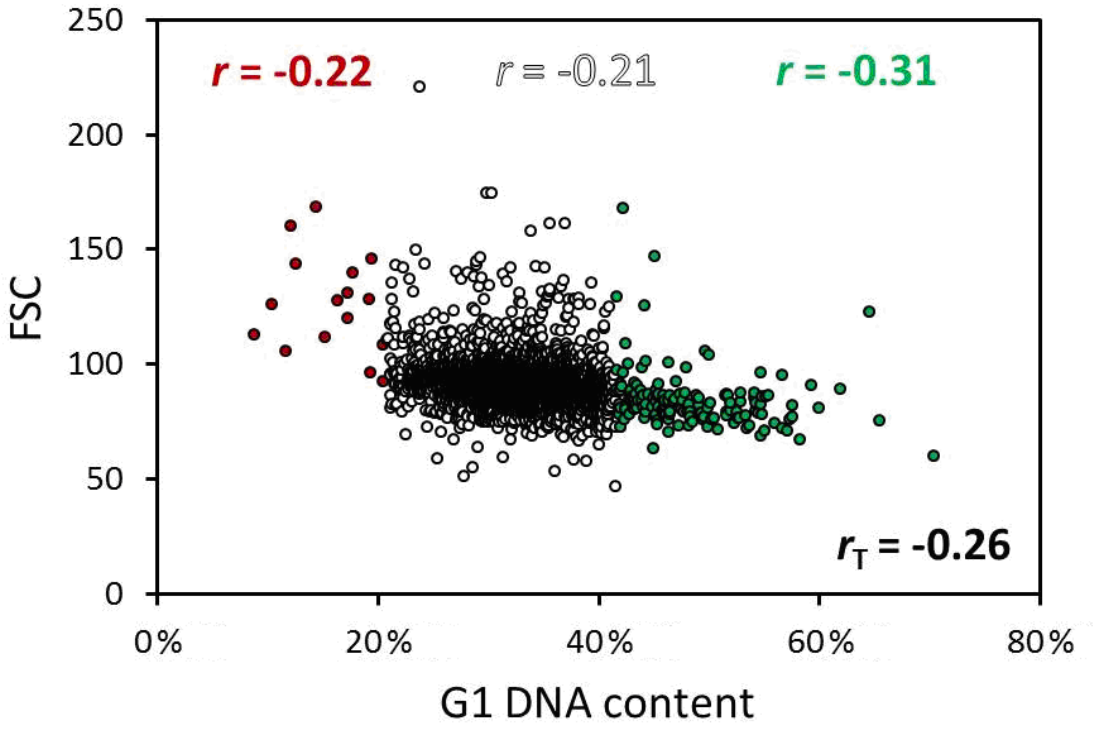

FIG A-5 Correlation between DNA content and FSC values. The %G1 is shown on the x-axis, and the forward angle scattering (FSC) values on the y-axis, from all the deletion strains we examined by flow cytometry. We calculated and displayed the *r* values as in Fig. 3. For every gene we included in this analysis, the values we used in this correlation are shown in Dataset C-1.

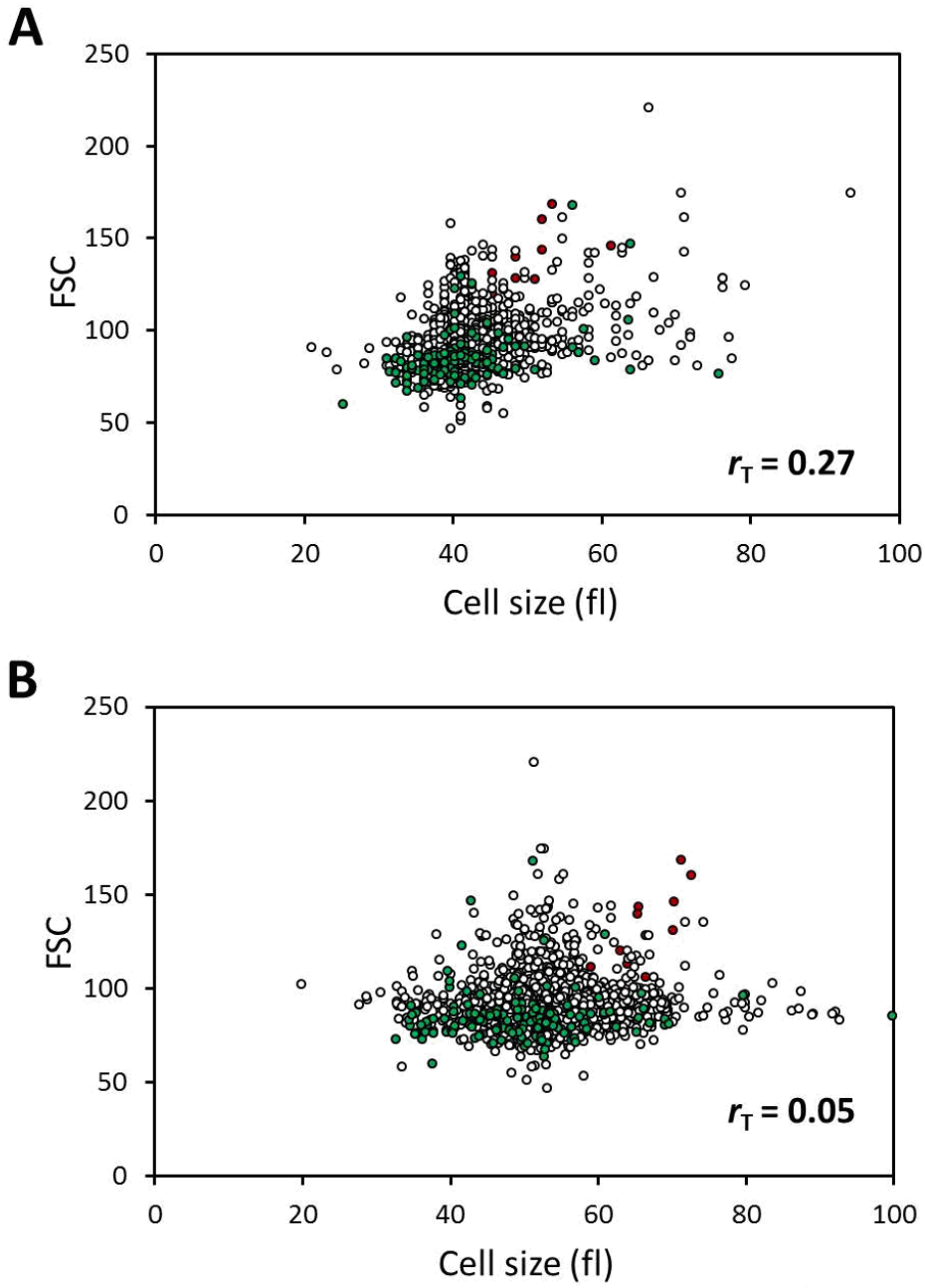

FIG A-6 Correlation between FSC and cell size values. We plotted the FSC values (y-axis) from all the deletion strains we examined against the median cell size (in fl, x-axis) data of Jorgensen et al (23) (A), or Zhang et al (24) (B). We calculated and displayed the *r* values as in Fig. 3. For every gene we included in this analysis, the values we used in this correlation are shown in Dataset C-1.

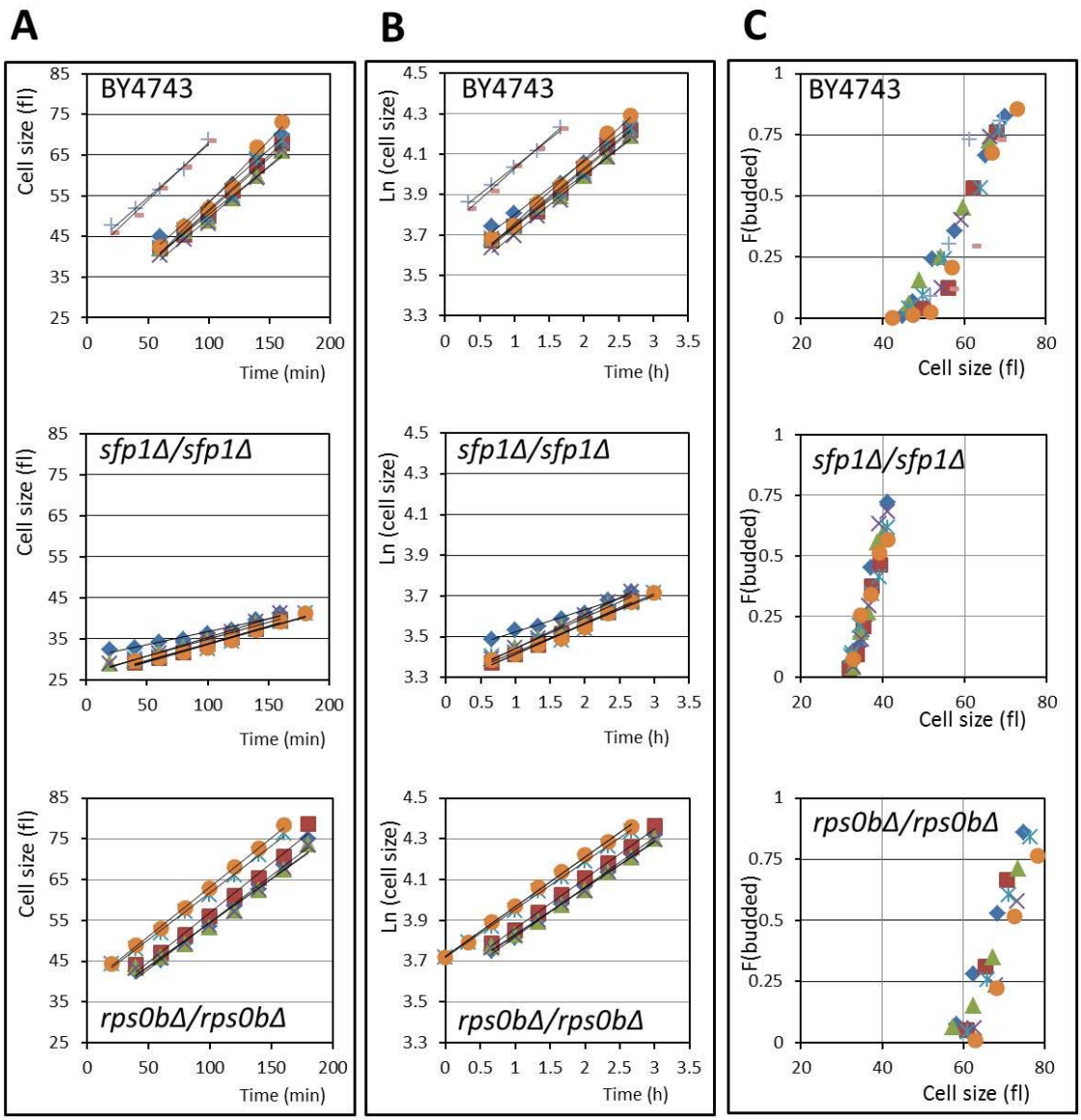

FIG A-7 Determining the timing of START in mutants that affect ribosome biogenesis. (A) Graphs from which we determined the rate of cell size increase shown in Fig. 5A, assuming linear growth. Our measurements were from synchronous cultures, in rich (YPD-2% Dextrose) medium. (B) Graphs from which we determined the specific rate of cell size increase constant *k*, shown in Fig. 5B, from the same elutriation experiments shown in A. In this case, we plotted the natural log of the cells size (y-axis), against time (shown in hours, x-axis). (C) Graphs of the fraction of budded cells (y-axis) as a function of cell size (in fl, x-axis), from the same elutriation experiments. The data points shown were from the linear portion of each experiment, when the percentage of budded cells began to increase, and used to determine the critical size for division we show in Fig. 5C.

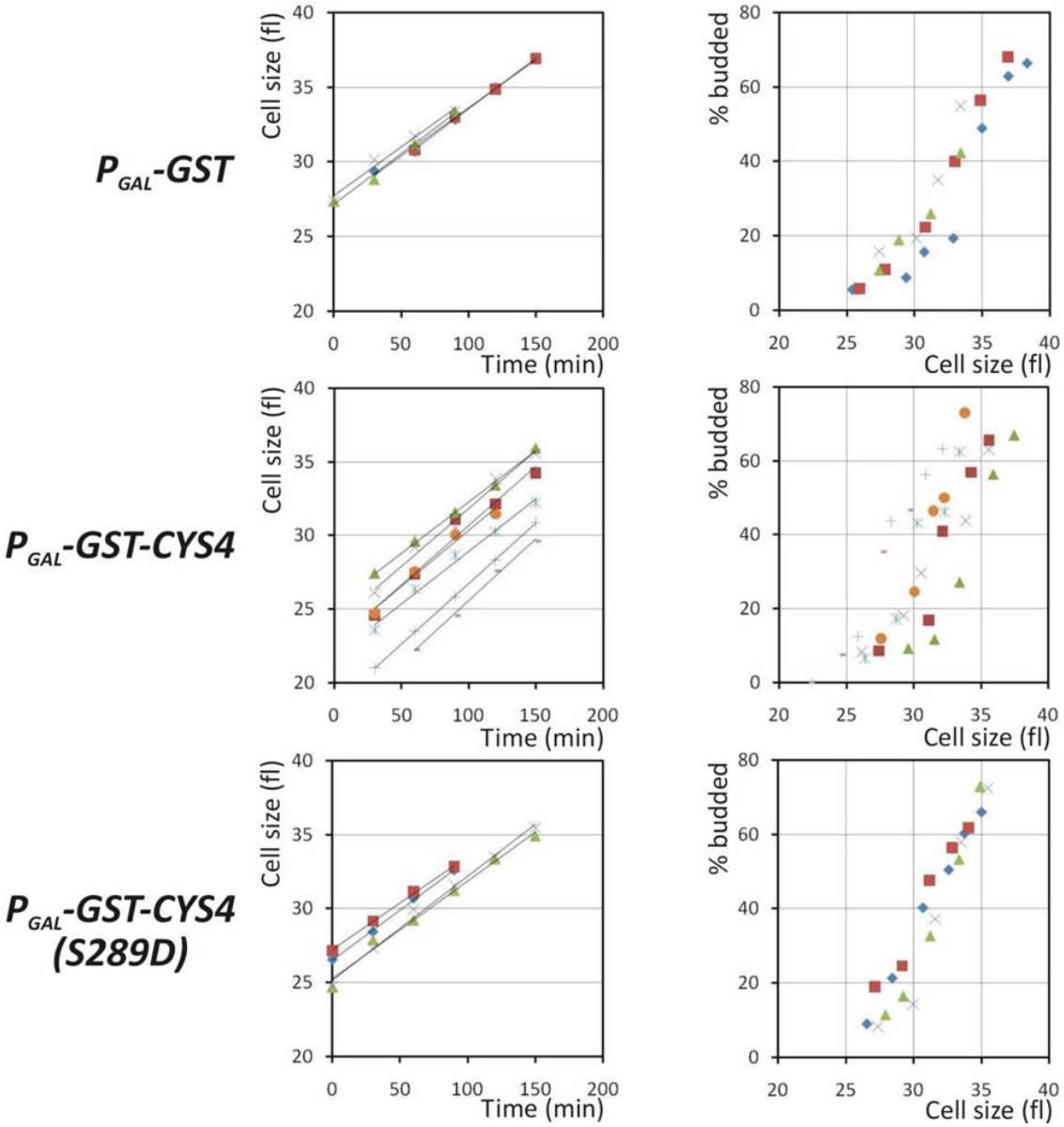

FIG A-8 Cell-cycle progression of synchronous cultures of P_{GAL} haploid strains, in galactose-containing media. The full data set used to calculate the values shown in Fig. 9A and 9B are shown on the left and right panels, respectively. Elutriations were done in media that contain galactose and induce expression of the P_{GAL} alleles (see Materials and Methods).

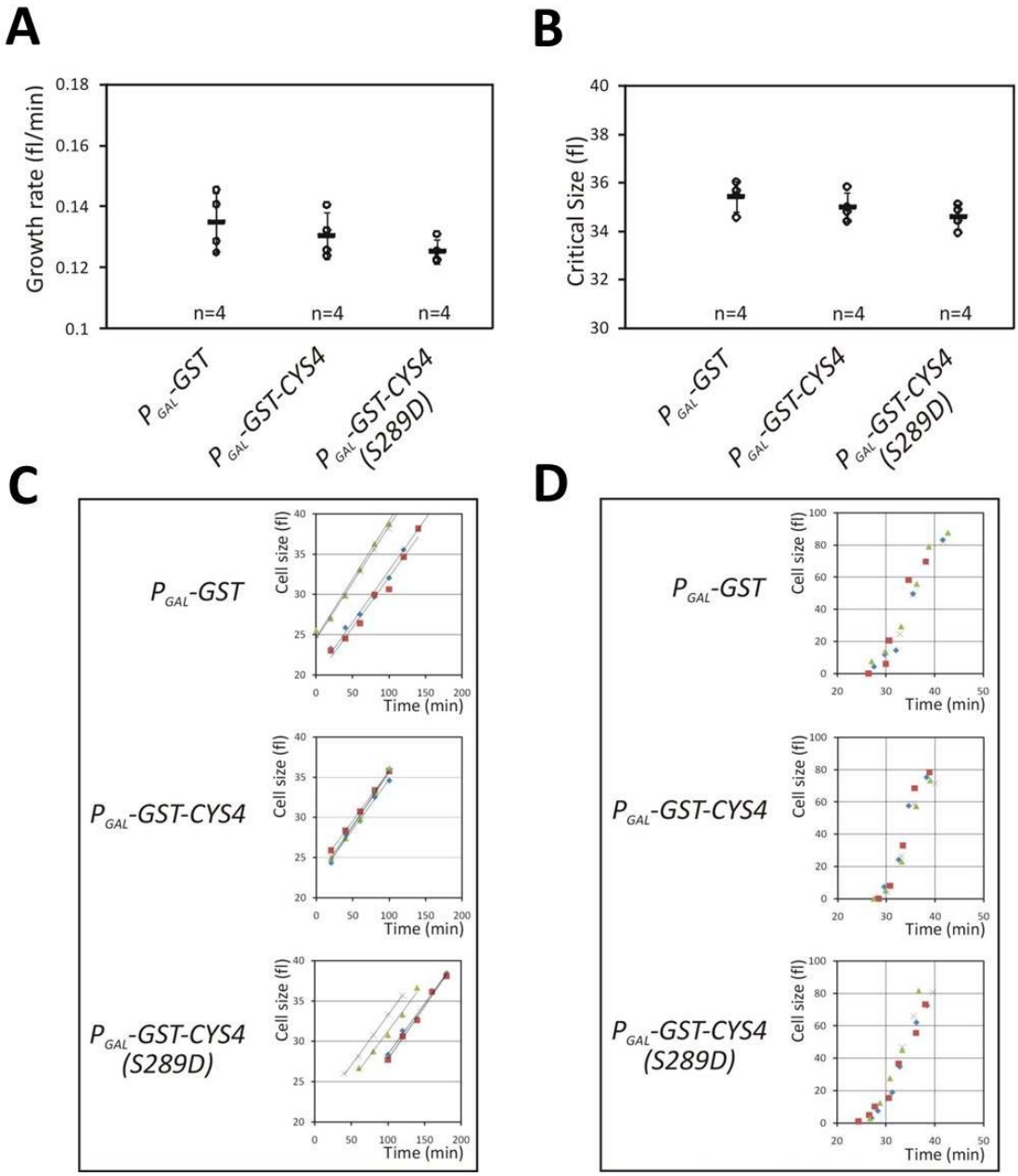

FIG A-9 Cell-cycle progression of synchronous cultures of P_{GAL} haploid strains, in repressive, glucose-containing media. (A) The rate of cell size increase (shown as growth rate, in fl/min) for the indicated strains was measured from synchronous elutriated cultures assuming linear growth, as in Fig. 9, in media that contain glucose (YPD-0.5% Dextrose) and repress expression of the P_{GAL} alleles. The average value for each strain is shown with a horizontal bar (± sd). (B) The critical cell size of the indicated strains (shown in fl), was measured from the same elutriation experiments shown in A. The rate of cell size increase for each elutriation experiment of the indicated strains is shown on the left panels. (C, D) The full data set used to calculate the values shown in A, and B, respectively.

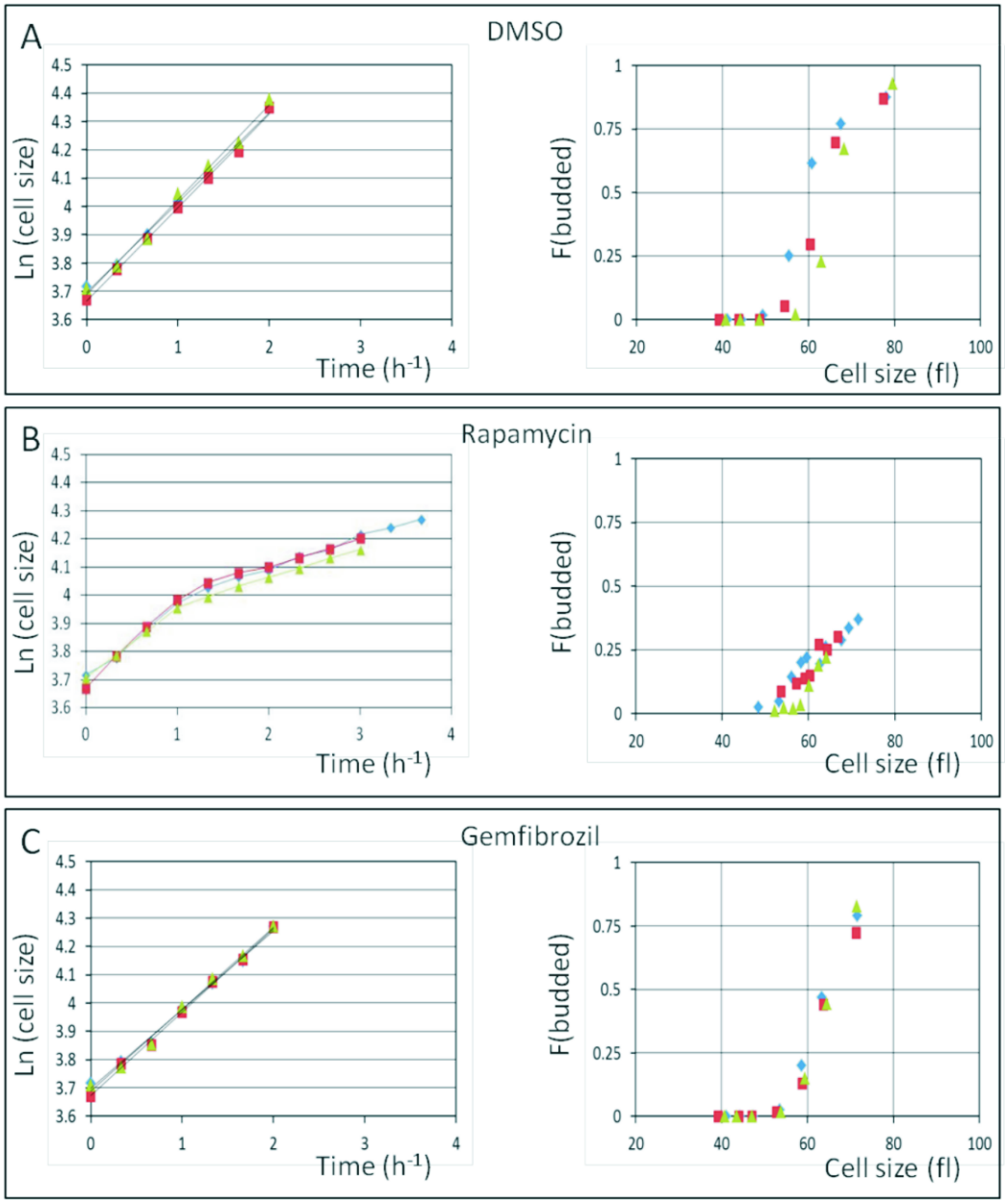

FIG A-10 Determining the length of G1. *Left*, Graphs from which we determined the specific rate of cell size increase constant *k*, shown in Fig. 15, from the same elutriation experiments. The natural log cell size (y-axis) is plotted against time (shown in hours, x-axis). *Right*, Graphs of the fraction of budded cells (y-axis) as a function of cell size (in fl, x-axis), from the same elutriation experiments. The data points shown were used to estimate the critical size for division we show in Fig. 15A. In (A) the cells were treated with DMSO, in (B) with rapamycin (at 0.1 μg/ml), and in (C) with gemfibrozil (at 50 μg/ml).

APPENDIX B

TABLES

TABLE B-1 *S. cerevisiae* strains used in this study

Strain	Genotype	Source
Homozygous diploid deletions (BY4743 background)	MATa/α *his3Δ1/his3Δ1 leu2Δ0 /leu2Δ0 lys2Δ0/LYS2 MET15/met15Δ0 ura3Δ0/ura3Δ0 orfΔ::kanMX4/orfΔ::kanMX4*	Research Genetics-Open Biosystems
W303-K699	MATa *ade2-1 ura3-1 trp1-1 can1-100 leu2-3, 112 his3-11, 15 GAL psi*$^{+}$	Bruce Futcher
SCSAH01	*ura3-1::P_{GAL}-GST::URA3 (at URA3)* (W303-K699 otherwise)	This study
SCSAH02	*ura3-1::P_{GAL}-GST-CYS4::URA3 (at URA3)* (W303-K699 otherwise)	This study
SCSAH03	*ura3-1::P_{GAL}-GST-CYS4(S289D)::URA3 (at URA3)* (W303-K699 otherwise)	This study
BY4742	MATa *his3Δ1 leu2Δ0 lys2Δ0 ura3Δ0*	Open Biosystems
16696	*cys4Δ::kanMX4* (BY4742 otherwise)	Open Biosystems
SCMSP178	*CYS4-13MYC::KanMX4* (BY4742 otherwise)	This study
SCMSP214	*CYS4(S289D)-13MYC::KanMX4* (BY4742 otherwise)	This study

TABLE B-2 Correspondence between genes that affect cell division when over-expressed, with genes required for normal cell-cycle progression

ORF	Phenotype		Comment
	Over-expression	Deletion	
YLR052W	G1		
YOR131C	G1		
YHL001W	G1	‡NA	
YER028C	G1		
YHR174W	G1	NA	
YDR117C	G1		
YGR112W	G1	G1	
YDR156W	G1		

ORF	Phenotype		Comment
	Over-expression	Deletion	
YCR046C	G1	†ND	
YDR493W	G1		
YOR065W	G1		
YPR152C	G1		
YDR397C	G1	NA	essential
YIR013C	G1		
YHL031C	G1	ND	
YPL127C	G1		
YHR070W	G1	NA	essential
YNL167C	G1	NA	
YMR275C	G1		
YGL105W	G1		
YLL066W-B	G1	NA	
YKL052C	G2	NA	essential
YBR131C-A	G2	NA	Dubious, overlaps YBR131W
YOR257W	G2	NA	essential
YCR093W	G2	NA	essential
YGR206W	G2		
YML055W	G2		
YHR172W	G2	NA	essential
YIL138C	G2		
YBL050W	G2	NA	essential
YOR326W	G2	NA	essential
YNL264C	G2		
YDR277C	G2		
YLR123C	G2		
YML052W	G2		
YHR014W	G2		
YHR002W	G2	NA	
YLR394W	G2		
YJR060W	G2	ND	
YCL026C-A	G2		
YPR015C	G2		
YOR286W	G2	ND	
YGR091W	G2	NA	essential
YDL002C	G2		

ORF	Phenotype		Comment
	Over-expression	Deletion	
YJL077W-A	G2	NA	Dubious, overlaps YJL077C
YML007W	G2		
YER145C	G2		
YLR149C	G2	ND	
YJL012C	G2		
YLR341W	G2		
YNL188W	G2	NA	essential
YOR195W	G2		
YGR109C	G2		
YBR211C	G2	NA	essential
YDR245W	G2		
YDR033W	G2		
YJL030W	G2		
YDR091C	G2	NA	essential
YIR001C	G2		
YKL078W	G2	NA	essential
YPR190C	G2	NA	essential
YDR266C	G2		
YDL214C	G2		
YDR001C	G2		
YIR016W	G2		
YBR083W	G2		
YKR067W	G2		
YHR131C	G2		
YFL022C	G2	NA	essential
YDR143C	G2		
YPL174C	G2	G1	*NIP100*
YOR002W	G2		
YNL283C	G2		
YPL247C	G2		
YJL031C	G2	NA	essential
YPR119W	G2	G2	*CLB2*
YML053C	G2		
YJL106W	G2		
YMR199W	G2		
YML016C	G2		

ORF	Phenotype		Comment
	Over-expression	Deletion	
YLR189C	G2		
YER007W	G2		
YEL022W	G2	NA	
YDL192W	G2		
YDR335W	G2		
YKR029C	G2		
YGR094W	G2	NA	essential
YBL031W	G2		
YGR005C	G2	NA	essential
YGR109W-A	G2	NA	Ty-transposon
YPL116W	G2		
YAR007C	G2	NA	essential
YDL093W	G2		
YOL063C	G2		
YJR125C	G2		
YIL036W	G2		
YOR337W	G2		
YOR007C	G2		
YJL128C	G2		
YIL158W	G2		
YHR177W	G2		
YGL066W	G2		
YMR068W	G2		
YER131W	G2		
YFL037W	G2	NA	essential
YDL155W	G2		
YPR120C	G2		
YFL039C	G2	NA	essential

‡NA, not available. These deletion strains were not in the panel.

†ND, not done. These deletion strains did not pass quality control either when they were generated, or when we analyzed them.

TABLE B-3 Correspondence between gene deletions that affect the budding index and the DNA content

ORF	Phenotype	
	BI*	%G1
YLR226W	Low	ND†
YKL068W	Low	
YHL025W	Low	High
YOR096W	Low	High
YJL089W	Low	
YHR008C	Low	ND
YLL007C	Low	
YHL011C	Low	High
YKR092C	Low	
YMR060C	Low	High
YCL058C	Low	High
YOR309C	Low	High
YPL257W	Low	
YPL240C	Low	
YPL271W	Low	High
YPL220W	Low	
YPL171C	Low	
YPL265W	Low	
YPL227C	Low	
YPL193W	Low	High
YPL226W	Low	High
YPL161C	Low	ND
YBR199W	Low	
YBR200W	Low	ND
YBR181C	Low	High
YPL125W	Low	High
YDR140W	Low	High
YDR379W	Low	
YDR418W	Low	High
YDR399W	Low	
YEL001C	Low	ND
YEL007W	Low	
YDR378C	Low	High
YKL009W	Low	High
YKL096W	High	
YKL113C	High	
YKL143W	High	

ORF	Phenotype	
	BI	%G1
YKL129C	High	
YOR107W	High	
YKL116C	High	
YKL164C	High	
YKL187C	High	
YOR279C	High	
YHR191C	High	
YJL047C	High	Low
YGR107W	High	
YPL267W	High	
YPL191C	High	
YPL120W	High	
YPL114W	High	
YPL108W	High	
YBR205W	High	
YBR231C	High	
YDR121W	High	ND
YDR122W	High	
YDR055W	High	
YDR073W	High	
YDR135C	High	
YDR085C	High	
YDR101C	High	
YDR069C	High	
YDR102C	High	
YDR338C	High	
YDR363W	High	
YDR369C	High	
YDR393W	High	
YDR402C	High	
YEL004W	High	
YCL016C	High	
YKL041W	High	
YKL048C	High	
YPR109W	High	
YPR115W	High	
YPR119W	High	Low
YPR135W	High	ND
YGR188C	High	

* BI, Budding Index, as defined in Zettel et al (119).
†ND, not done.

TABLE B-4 Gene Ontology Enrichment of the "Low G1" group*

ID	Process	p-value
GO:0022403	cell cycle phase	0.0017
GO:0010529	negative regulation of transposition	0.0052
GO:0033554	cellular response to stress	0.0104
GO:0006974	response to DNA damage stimulus	0.0316
GO:0007049	cell cycle	0.0426
GO:0000278	mitotic cell cycle	0.0438
GO:0000725	recombination repair	0.0464

* The analysis was performed with the YeastMine (v. 2011-10-09) feature of the Saccharomyces Genome Database (http://yeastmine.yeastgenome.org/yeastmine).

TABLE B-5 Gene Ontology Enrichment of the "High G1" group*

ID	Process	p-value
GO:0002181	cytoplasmic translation	$2.56E^{-17}$
GO:0042274	ribosomal small subunit biogenesis	$9.35E^{-15}$
GO:0042254	ribosome biogenesis	$2.24E^{-13}$
GO:0022613	ribonucleoprotein complex biogenesis	$1.01E^{-12}$
GO:0030490	maturation of SSU-rRNA	$3.05E^{-11}$
GO:0071843	cellular component biogenesis at cellular level	$3.58E^{-10}$
GO:0000462	maturation of SSU-rRNA from tricistronic rRNA transcript (SSU-rRNA, 5.8S rRNA, LSU-rRNA)	$1.15E^{-09}$
GO:0044085	cellular component biogenesis	$1.10E^{-07}$
GO:0006364	rRNA processing	$1.68E^{-06}$
GO:0016072	rRNA metabolic process	$3.71E^{-06}$
GO:0006412	translation	$3.81E^{-06}$
GO:0042255	ribosome assembly	$3.07E^{-05}$
GO:0034470	ncRNA processing	$5.04E^{-05}$
GO:0000028	ribosomal small subunit assembly	$1.13E^{-04}$
GO:0070925	organelle assembly	$1.59E^{-04}$
GO:0006396	RNA processing	$2.57E^{-04}$
GO:0034660	ncRNA metabolic process	$8.03E^{-04}$
GO:0071841	cellular component organization or biogenesis at cellular level	0.0017

ID	Process	p-value
GO:0022618	ribonucleoprotein complex assembly	0.0035
GO:0007035	vacuolar acidification	0.0053
GO:0045851	pH reduction	0.0053
GO:0051452	intracellular pH reduction	0.0053
GO:0071826	ribonucleoprotein complex subunit organization	0.0056
GO:0006407	rRNA export from nucleus	0.0070
GO:0030641	regulation of cellular pH	0.0070
GO:0051029	rRNA transport	0.0070
GO:0051453	regulation of intracellular pH	0.0070
GO:0071840	cellular component organization or biogenesis	0.0113
GO:0006885	regulation of pH	0.0193
GO:0000478	endonucleolytic cleavage involved in rRNA processing	0.0270
GO:0000479	endonucleolytic cleavage of tricistronic rRNA transcript (SSU-rRNA, 5.8S rRNA, LSU-rRNA)	0.0270
GO:0010467	gene expression	0.0407
GO:0015931	nucleobase, nucleoside, nucleotide and nucleic acid transport	0.0417
GO:0050658	RNA transport	0.0495
GO:0051236	establishment of RNA localization	0.0495

***** The analysis was performed with the YeastMine (v. 2011-10-09) feature of the Saccharomyces Genome Database (http://yeastmine.yeastgenome.org/yeastmine).

TABLE B-6 Drugs that lead to a High G1 DNA content

Drug	***%G1***	***Use‡***	***Type***
Auranofin†	95.94%	Antirheumatic	Organogold compound
Ketoconazole	84.05%	Antifungal	Ergosterol inhibitor
Climbazole	83.30%	Antifungal	Ergosterol inhibitor
Oxatomide	79.10%	Antiallergic, antiasthmatic	Histamine H1 antagonist
Rapamycin	78.81%	Immunosuppressant, anticancer	TOR inhibitor
Myclobutanil	76.56%	Antifungal	Ergosterol inhibitor
Aripiprazole	76.24%	Antipsychotic	Presynaptic dopamine agonist, postsynaptic D2 antagonist
Haloperidol	76.21%	Antipsychotic	Dopamine antagonist
Flunarizine	76.11%	Antimigraine	Calcium channel blocker

Drug	*%G1*	*Use‡*	*Type*
Itraconazole	75.14%	Antifungal	Ergosterol inhibitor
Gestrinone	73.60%	Contraceptive	Steroid
Clopidogrel	71.92%	Platelet aggregation inhibitor	
Dehydroepi-androsterone	71.86%		Steroid
Fluconazole	71.14%	Antifungal	Ergosterol inhibitor
Nystatin	69.94%	Antifungal	Ionophore
Ibudilast	69.85%	Vasodilator	Phosphodiesterase inhibitor
Lovastatin	69.77%	Anticholesteremic	HMG-CoA reductase inhibitor
Ifenprodil	69.36%	Anticonvulsant, vasodilator	NMDA receptor inhibitor
Progesterone	69.33%		Steroid
Vatalanib	69.08%	Antiangiogenic	Protein kinase inhibitor
Artemisinin	69.05%	Antimalarial	
Nefazodone	68.80%	Antidepressant	
Fenretinide	68.11%	Antineoplastic	Retinoid
Amlodipine	67.31%	Antihypertensive, vasodilator	Calcium channel blocker
Gemfibrozil	66.69%	Antilipemic	PPARa activator
Alfacalcidol	65.06%	Bone density conservation	Vitamin D analog
Canrenone	64.94%		Steroid

‡Information about the use and type for each drug was obtained from PubChem (http://pubchem.ncbi.nlm.nih.gov/).
†Drugs shown in bold were active both in *pdr5Δ, snq2Δ*, and in *PDR5*$^{+}$ *SNQ2*$^{+}$ cells.

TABLE B-7 Drugs that lead to a Low G1 DNA content

Drug	*%G1*	*Use‡*	*Type*
Fluoxetine†	16.98%	Antidepressant	Serotonin uptake inhibitor
Promethazine	20.39%	Antiallergic	Histamine H1 antagonist
Moxifloxacin	21.17%	Antimicrobial	Topoisomerase inhibitor
Clinafloxacin	25.38%	Antimicrobial	Topoisomerase inhibitor
Mitomycin c	27.26%	Antineoplastic	Alkylating agent
Chlorpromazine	27.80%	Antipsychotic	Dopamine antagonist
Nadifloxacin	28.13%	Antimicrobial	Topoisomerase inhibitor
Idarubicin	29.10%	Antineoplastic	Intercalating agent

Drug	*%G1*	*Use‡*	*Type*
Clozapine	31.90%	Antipsychotic	GABA and Serotonin antagonist
Gatifloxacin	33.52%	Antimicrobial	Topoisomerase inhibitor
Aclarubicin	36.42%	Antineoplastic	Intercalating agent
Sparfloxacin	36.57%	Antimicrobial	Topoisomerase inhibitor

‡Information about the use and type for each drug was obtained from PubChem (http://pubchem.ncbi.nlm.nih.gov/).
†Drugs shown in bold were active both in *pdr5Δ, snq2Δ*, and in $PDR5^{+}$ $SNQ2^{+}$ cells.

TABLE B-8 Fluoxetine strongly inhibits yeast cell proliferation, but it is suppressed by gemfibrozil

	[Gemfibrozil]			
[Fluoxetine]	**0 µM**	**50 µM**	**100 µM**	**200 µM**
0 µM	0.41±0.03*	0.43±0.01	0.45±0.01	0.40±0.01
50 µM	0.41±0.02	0.43±0.01	0.45±0.00	0.42±0.02
100 µM	0.39±0.02	0.45±0.01	0.47±0.00	0.43±0.01
200 µM	0.03±0.01	0.46±0.02	0.44±0.03	0.42±0.01

*The specific growth rate constant (*k*) of each drug combination is shown. These values were used to generate the graph in Fig. 16A. Errors represent the standard deviation of nine replicates of the 0 µM/0 µM control, and ranges of two replicates of all others.

TABLE B-9 Gemfibrozil suppresses fluoxetine's anti-proliferative effects only if added before, but not after, fluoxetine

	2nd treatment		
1st treatment	**DMSO**	**Gemfibrozil**	**Fluoxetine**
DMSO	0.470±0.001*	0.400±0.002	0.108±0.005
Gemfibrozil	0.475±0.006	0.402±0.001	0.277±0.004
Fluoxetine	0.287±0.001	0.239±0.001	-0.008±0.001

*The specific growth rate constant (*k*) of each treatment combination is shown. These values were used to generate the graph in Fig. 16B. Errors represent the ranges of two replicates for all samples.

APPENDIX C

ATTACHED DATASETS

Description of attached MS Excel files:

Dataset C-1.xls. (4.04 MB) Searchable spreadsheet of all the primary gene deletion data analysis, arranged in different worksheets. In the worksheet entitled "Data and Correlation", we list the experimental data we obtained, representing mean average values for individual deletions, organized by plate ID. Data from our study are correlated to growth and cell size data from the indicated studies, and descriptions from the Saccharomyces Genome Database (SGD; http://www.yeastgenome.org/). In the worksheet entitled "INCLUDED Experiments", we list all our flow cytometry individual experiments that were included in the final analysis. Raw .fcs files can be accessed at Cytobank (www.cytobank.org). Public experiment name: "Yeast DNA Content Project – DELETION – INCLUDED". In the worksheet entitled "EXCLUDED Experiments", we list individual experiments that were excluded from the final analysis for various reasons, but which may represent valid flow cytometry profiles. Cytobank public experiment name: "Yeast DNA Content Project – DELETION – EXCLUDED". Finally, in the worksheet entitled "Explanation", we provide further detailed descriptions of each parameter listed in the previous worksheets.

Dataset C-2.xlsx. (503 KB) Searchable spreadsheet of all the primary drug treatment data analysis, arranged in different worksheets. Layout and formatting is similar to that of Dataset C-1. Raw .fcs files can be accessed at Cytobank (www.cytobank.org). Public experiment names: "Yeast DNA Content Project – DRUG – INCLUDED" and "Yeast DNA Content Project – DRUG – EXCLUDED".

VITA

Name: Scott Allen Hoose

Address: Department of Biochemistry and Biophysics
College of Agriculture and Life Sciences
Texas A&M University
2128 TAMU
College Station, TX 77843-2128

Email address: hoose@tamu.edu

Education: B.A., Biology, Texas A&M University, College Station

Recent publications:

Hoose SA, Duran C, Malik I, *et al*. Systematic analysis of cell cycle effects of common drugs leads to the discovery of a suppressive interaction between gemfibrozil and fluoxetine. *PLoS One*. 2012 7(5): e36503

Hoose SA, Rawlings JA, Kelly MM, *et al*. A systematic analysis of cell cycle regulators in yeast reveals that most factors act independently of cell size to control initiation of division. *PLoS Genet.* 2012 Mar;8(3):e1002590. Epub 2012 Mar 15.

Henry KA, Blank HM, **Hoose SA**, Polymenis M. The unfolded protein response is not necessary for the G1/S transition, but it is required for chromosome maintenance in Saccharomyces cerevisiae. *PLoS One*. 2010 Sep 14;5(9):e12732.

Qi R, **Hoose S**, Schreiter J, *et al*. Secretion of the human Toll-like receptor 3 ectodomain is affected by single nucleotide polymorphisms and regulated by Unc93b1. *J Biol Chem*. 2010 Nov 19;285(47):36635-44. Epub 2010 Sep 20.

Pardo C, **Hoose SA**, Pondugula S, Kladde MP. DNA methyltransferase probing of chromatin structure within populations and on single molecules. *Methods Mol Biol.* 2009;523:41-65.

Ranjith-Kumar CT, Duffy KE, Jordan JL, *et al*. Single-stranded oligonucleotides can inhibit cytokine production induced by human toll-like receptor 3. *Mol Cell Biol*. 2008 Jul;28(14):4507-19. Epub 2008 May 19.

Ranjith-Kumar CT, Miller W, Sun J, *et al*. Effects of single nucleotide polymorphisms on Toll-like receptor 3 activity and expression in cultured cells. *J Biol Chem.* 2007 Jun 15;282(24):17696-705. Epub 2007 Apr 13.